RESEARCH ARTICLE

Key Points:

- Several convection schemes were tested via two recently proposed, idealized experiments designed to isolate memory-like behavior
- All schemes either fail to show any such behavior, or show weaker memory than an explicit cloud-resolving model
- By fitting simple equation sets to the results, structural assumptions and parameters related to subgrid memory processes can be constrained

Correspondence to:
Y.-L. Hwong,
yiling.hwong@gmail.com

Author Contributions:
Conceptualization: Y.-L. Hwong, M. Colin, S. C. Sherwood
Formal analysis: Y.-L. Hwong
Funding acquisition: C. J. Muller, S. C. Sherwood
Investigation: Y.-L. Hwong, M. Colin, C. J. Muller
Methodology: Y.-L. Hwong, M. Colin, S. C. Sherwood
Project Administration: C. J. Muller, S. C. Sherwood
Supervision: C. J. Muller, S. C. Sherwood
Validation: M. Colin

Assessing Memory in Convection Schemes Using Idealized Tests

Y.-L. Hwong[1] ⓘ, M. Colin[2,3] ⓘ, P. Aglas-Leitner[1], C. J. Muller[1], and S. C. Sherwood[3] ⓘ

[1]Institute of Science and Technology Austria, Klosterneuburg, Austria, [2]Complexity and Climate, Leibniz Centre for Tropical Marine Research, Bremen, Germany, [3]Climate Change Research Centre, University of New South Wales, Sydney, NSW, Australia

Abstract Two assumptions commonly applied in convection schemes—the diagnostic and quasi-equilibrium assumptions—imply that convective activity (e.g., convective precipitation) is controlled only by the large-scale (macrostate) environment at the time. In contrast, numerical experiments indicate a "memory" or dependence of convection also on its own previous activity whereby subgrid-scale (microstate) structures boost but are also boosted by convection. In this study we investigated this memory by comparing single-column model behavior in two idealized tests previously executed by a cloud-resolving model (CRM). Conventional convection schemes that employ the diagnostic assumption fail to reproduce the CRM behavior. The memory-capable *org* and Laboratoire de Météorologie Dynamique Zoom cold pool schemes partially capture the behavior, but fail to fully exhibit the strong reinforcing feedbacks implied by the CRM. Analysis of this failure suggests that it is because the CRM supports a linear (or superlinear) dependence of the subgrid structure growth rate on the precipitation rate, while the *org* scheme assumes a sublinear dependence. Among varying versions of the *org* scheme, the growth rate of the *org* variable representing subgrid structure is strongly associated with memory strength. These results demonstrate the importance of parameterizing convective memory, and the ability of idealized tests to reveal shortcomings of convection schemes and constrain model structural assumptions.

Plain Language Summary Convection (clouds) has memory, can remember its own history, and is affected by it when evolving to the next step. However, this memory effect is often neglected in convection schemes, which are approximate sub-models used to represent (parameterize) convective processes in climate models whose resolutions are too low to properly resolve convection. In this study we apply two simple tests to probe the memory behavior of various convection schemes. We found that most conventional schemes fail to mimic the memory response of a cloud-resolving model (CRM) where convection is properly represented. In two schemes where memory is parameterized, their responses are more similar but still bear significant differences to the CRM. We show that this discrepancy can be explained by the equations used in these schemes. For one of the schemes, we also found that the strength of memory is related to the growth rate of the memory variable, rather than its absolute value. Overall, our results demonstrate the importance of taking memory into account in convection schemes, and show that the two tests implemented here are simple but useful in shining light on potential shortcomings of convection schemes and hence also ways to improve them.

1. Introduction

Cumulus convection is a key process in tropical climate dynamics and plays a crucial role in transporting and redistributing momentum, heat and moisture in the atmosphere. It is a complex process that involves a multitude of time and spatial scales. In general circulation models (GCMs), the impact of unresolved convective processes on resolved scales is accomplished through parameterization. Despite great strides in recent years (Rio et al., 2019; Villalba-Pradas & Tapiador, 2022), convective parameterization remains an important source of uncertainty in GCMs (Stephens et al., 2010; Stevens & Bony, 2013).

Two structural assumptions commonly applied in convection schemes and relevant to the present study are the diagnostic and quasi-equilibrium assumptions. The former states that convective activity at any given instant can be determined using solely the resolved grid-scale variables at that instant via an unspecified function (typically different in different schemes) and that there is no conditional dependence of convection on its own history beyond that projected by the resolved variables. The latter assumes that convective instability

10.1029/2023MS003726

Visualization: Y.-L. Hwong, M. Colin, P. Aglas-Leitner, C. J. Muller
Writing – original draft: Y.-L. Hwong, M. Colin
Writing – review & editing: Y.-L. Hwong, M. Colin, P. Aglas-Leitner, C. J. Muller, S. C. Sherwood

generated by slowly-evolving large-scale forcing is quickly consumed by fast-acting convective processes and is commonly used as a closure assumption in convection schemes (Arakawa & Schubert, 1974; Yanai et al., 1973; Yano & Plant, 2012). However, both assumptions do not fully capture what happens in reality because convection takes a finite time to adjust to large-scale forcing (Arakawa & Schubert, 1974; Pan & Randall, 1998), and is affected by pre-existing convection (Davies et al., 2009, 2013). The fact that convection has inertia, can feel the influence of its own activity at an earlier time, and is modified by it, is termed the "memory" of convection (Davies et al., 2009). Its parameterization is the focus of this study.

It is important to differentiate between two types of memory that have been identified in cloud-resolving model (CRM) studies: macro- and microstate memories (Colin et al., 2019, henceforth C19). We refer to the memory effects arising from a changing large-scale ("macrostate") environment as "macrostate memory." In the context of parameterization, it represents the impact of processes that affect the mean profiles of a single GCM grid cell over a finite time, relaxing the quasi-equilibrium assumption. It is commonly taken into account in convection schemes via a finite "adjustment time scale" of 1–5 hr (Bechtold et al., 2008; Cohen & Craig, 2004; Kain, 2004; Xu & Randall, 1998). In this study we are interested in another memory, which emerges due to small-scale ("microstate") structures or heterogeneities within a GCM grid box (or within a CRM domain), and is produced by but also promotes convection, the so-called "microstate memory" (C19). These structures could arise as a consequence of individual clouds changing their surroundings during their lifespans and manifest themselves as remnants of past convective activity influencing the development of convection at the present time (Davies et al., 2009, 2013). This type of memory arises from subgrid-scale processes that remain unresolved in GCMs (but resolved in CRMs) and must therefore be parameterized. To avoid confusion, memory refers to microstate memory in the present study. Although they resolve subgrid-scale processes better than GCMs, the manifestation of memory may vary between CRMs. Convective memory has been shown to be strongly associated with convective organization (C19; Davies, 2008; Moseley et al., 2016), and the degree of organization displayed across different CRMs is far from uniform (Wing et al., 2020). Within a single CRM, convective organization has been found to be sensitive to domain size and horizontal resolution (Muller & Held, 2012; Yanase et al., 2020), but this dependence disappears when rain evaporation is removed in the boundary layer (Jeevanjee & Romps, 2013; Muller & Bony, 2015). Nonetheless, CRMs display more consistency in their organization behavior compared to GCMs (Wing et al., 2020), and hence their memory behavior can also be expected to be more accurate than parameterized convection.

Multiple CRM studies have shown that memory mainly resides in low-level thermodynamic inhomogeneities. These studies involve simulations conducted under radiative-convective equilibrium (RCE) conditions (a statistical equilibrium state of the atmosphere where radiative cooling is balanced by convective heating, reminiscent of conditions in the tropical atmosphere over ocean) (C19; Davies et al., 2013), as well as more realistic scenarios with an imposed diurnal cycle (Daleu et al., 2020). Two of these CRM studies are relevant to our analysis. To identify memory and its effects, C19 imposed an instantaneous homogenization of the microstate structures (setting a given subset of prognostic variables to their domain-averaged values) and observed how convective activity (precipitation) recovered after this homogenization. They found that memory is predominantly contributed by the water vapor and temperature microstructures (variability) in the subcloud layer compared to winds and hydrometeors. A longer recovery time scale was observed when convection is organized (>24 hr) than when disorganized (2–3 hr). A follow-up study by Colin and Sherwood (2021, henceforth CS21) explored the memory behavior of a CRM when the macrostate is held fixed to its equilibrium mean state ("strong-nudging" experiment). In this case convection displays a volatile behavior, with precipitation either growing exponentially to an unrealistically large value or decaying to zero. Additionally, the authors presented a two-variable, predator-prey (PP) model that was able to capture this instability, as well as the CRM behavior in C19's homogenization experiment. Further description of the PP model is presented in Section 3.3.

In CRM simulations, physical mechanisms that contribute to the spatial variance of the vertically integrated moist static energy (MSE) have been found to be strongly correlated with convective organization (Wing & Emanuel, 2014) and hence memory (C19). There are many such processes but we focus on one that is of particular importance to the present study: the evaporation of rain. By injecting cooler and drier air into the boundary layer, which is then preferentially excluded from convective updrafts, rain evaporation increases the horizontal variation in the planetary boundary layer (PBL) thermodynamic conditions. Indeed, myriad CRM studies have found rain evaporation to impact convective organization under idealized RCE (Holloway & Woolnough, 2016; Jeevanjee & Romps, 2013; Muller & Bony, 2015) as well as more realistic conditions (Holloway, 2017). Cold

pools produced by the evaporation of rain are also well-known to have a profound impact on convective organization by influencing the thermodynamic stability of the PBL (Tompkins, 2001; Torri & Kuang, 2016; Zuidema et al., 2017) and playing a crucial role in the dynamic triggering of convection (Haerter et al., 2019; Torri et al., 2015). Despite the knowledge gained from CRM experiments it remains unclear how memory should be parameterized, and a wide range of approaches have been attempted. These include the introduction of prognostic variables that influence the evolution of various scheme calculations such as entrainment (Mapes & Neale, 2011, henceforth MN11), closure formulation (Pan & Randall, 1998; Randall & Pan, 1993), updraft area fraction (Gerard et al., 2009), updraft and downdraft (Tan et al., 2018), convective vertical velocity (Guérémy, 2011), microphysics (Piriou et al., 2007); the explicit modeling of physical processes such as cold pools (Del Genio et al., 2015; Grandpeix & Lafore, 2010; Park, 2014a, 2014b; Qian et al., 1998; Rooney et al., 2022), cloud lifecycles (Sakradzija et al., 2015, 2016), evolution of thermal clusters (Neggers & Griewank, 2021, 2022); the use of Markov chains (Hagos et al., 2018; Khouider et al., 2010; Peters et al., 2013) and cellular automata (Bengtsson et al., 2013, 2021); the adoption of machine learning algorithms such as convolutional and recurrent neural networks to capture temporal dependencies (Caseri et al., 2022; Y. Han et al., 2020; Shamekh et al., 2023); and embedding CRM in GCM grid cells through super-parameterization (Khairoutdinov et al., 2005; Khairoutdinov & Randall, 2001; Pritchard et al., 2011). Given the immense diversity in memory parameterizations, we deem it an important task to design tests in a simple and intuitive framework to probe the behavior and potentially reveal the shortcomings of current schemes. It is therefore the goal of this paper to examine two convection schemes with memory using two idealized tests.

The first convection scheme that we tested is the UW-*org* scheme, which we briefly describe here and refer to MN11 for in-depth details. The scheme is based on the University of Washington (UW) shallow convection scheme implemented in the Community Atmosphere Model (CAM5), which is a single-plume mass flux scheme (Park & Bretherton, 2009). The modified UW-*org* scheme is conceptualized as a unified (shallow and deep) scheme. Memory is parameterized via the introduction of a new prognostic *org* variable meant to capture the effects of subgrid-scale structures on convective processes such as entrainment rate and closure. In particular, entrainment rate has been found to have an impact on convective organization, and vice versa (Becker et al., 2018; Tompkins & Semie, 2017). To be clear, although the variable *org* can be expected to represent certain aspects of convective organization, it is not necessarily so and should be more accurately interpreted as a representation of heterogeneities in the MSE fields that could contribute to positive feedback on the development of convection, and hence to memory. While an arbitrary number of plumes can be computed, the current implementation contains only two plumes that are computed sequentially, and whose mass fluxes and area coverages are combined to determine the total precipitation and other convective tendencies. Entrainment rates and plume base conditions (temperature and humidity) may differ between the plumes, and thus may also the heights the plumes reach. *Org* is a 2D, dimensionless variable whose prognostic equation is given by

$$\frac{\mathrm{d}(org)}{\mathrm{d}t} = S - \frac{(org)}{\tau_{org}} \tag{1}$$

where S is the source of *org* (defined as the mass-weighted vertically integrated rain evaporation rate in kg m^{-2} s^{-1} times *evap2org*, an adjustable parameter) and τ_{org} its characteristic time scale. Following MN11, we set *evap2org* to 2 m^2 kg^{-1} and τ_{org} to 10 ks (~3 hr). We elaborate further on the effects of *org* on entrainment rate and closure in Section 2.2.

The second scheme we tested is the cold pool (CP) scheme in the Laboratoire de Météorologie Dynamique Zoom (LMDZ) model (Grandpeix & Lafore, 2010), the atmospheric component of the Institut Pierre-Simon Laplace model. This scheme represents spreading circular cold pools fed by precipitation evaporation in unsaturated downdrafts. Their dynamics follows that of a density current: they convert gravitational potential energy into kinetic energy. These cold pools impact convection in three ways. First, their negative buoyancy provides energy to trigger deep convection via mechanical lifting. Second, cold pool edges act as gust fronts and provide power for the convective closure via an Available Lifting Power (ALP), which is proportional to total cold pool perimeter and increases with cold pool spread speed. Third, cold pools create two subgrid-scale environments: the colder cold pool environment seen by downdrafts, and the warmer exterior seen by updrafts in the convection scheme. The cold pools are prognostic, and their memory comes from their density current properties. The prognostic memory variables are the cold pool temperature and humidity anomalies, as well as the total cold pool surface area. A summary of the main cold pool governing equations is presented in Grandpeix et al. (2010).

The overarching goal of this study is to examine and improve understanding of the memory behavior of the UW-*org* and LMDZ-CP schemes by using a single-column model (SCM) setup under RCE conditions and comparing their responses to those of previously published CRM RCE results (C19 and CS21). The specific research questions addressed are:

1. How do convection schemes respond when we fix the large-scale environment, that is, disable the feedback between micro- and macrostates?
2. How do convection schemes respond when we homogenize their microstate structures carrying memory?
3. How do their above responses compare to those of (a) schemes with no microstate memory, and (b) a CRM where convection is resolved?

There is a long tradition of using SCMs to evaluate the performance of physics parameterization by comparing their results to those of CRMs or large-eddy simulations, commonly by prescribing both models with large-scale forcings derived from GCM outputs or observations (e.g., Bretherton, McCaa, & Grenier, 2004; Dal Gesso & Neggers, 2018; Gettelman et al., 2019; Rio et al., 2010). The obvious caveat of using SCMs in this way is the absence of feedback between model physics and large-scale circulations, which limits the interpretation of results, given that convection schemes are coupled to model dynamics in 3D simulations. Under RCE conditions, however, there is no lateral energy transport and large-scale vertical motion is assumed to be zero, hence removing the need for imposed large-scale dynamics. By isolating the effects of model physics, SCMs in RCE are therefore a simple yet intuitive setup to assess convective parameterization (Jeevanjee et al., 2017).

2. Methods

2.1. Models and Simulation Setup

Two models in their SCM setup were used in this study: the Weather Research and Forecasting (WRF) and LMDZ models. For WRF, the SCM test case was used (*em_scm*; WRF version 4.0.2; Skamarock et al., 2019). For LMDZ, the LMDZ5B+ version was used, which is based on the CMIP5 version (LMDZ5B; Hourdin et al., 2013) but with additional developments (revision 2420). As reference we used previously published WRF CRM results (see C19 and CS21). The CRM uses the Advanced Research WRF fully compressible, Eulerian non-hydrostatic solver (version 3.6; Skamarock et al., 2008). The CRM simulations have 202×202 grid points, with a horizontal resolution of 1 km. For a full description of the CRM setup we refer readers to C19 and CS21.

The SCM control simulations were conducted under RCE conditions over an ocean surface, with a fixed sea surface temperature of 302 K. In WRF SCM, a stretched vertical grid spacing with 74 model levels was used, with model bottom and top at around 40 m and 33 km, respectively. In LMDZ, another stretched vertical grid spacing was used, with 79 vertical levels, ranging from 10 m to 80 km.

In terms of convective parameterization, for this study we have imported into WRF the UW-*org* scheme originally developed for the CAM5 model. We also tested in WRF five standard convection schemes without memory: the Zhang-McFarlane (ZM; G. Zhang & McFarlane, 1995), Kain-Fritsch (KF; Kain, 2004), New-Tiedtke (NT; C. Zhang & Wang, 2017), New-Simplified Arakawa-Schubert (NSAS; J. Han & Pan, 2011), and Betts-Miller-Janjic (BMJ; Betts, 1986; Betts & Miller, 1986; Janjić, 1994) schemes. The LMDZ SCM uses a modified version of the mass flux deep convection scheme of Emanuel (1991) and Emanuel and Živković-Rothman (1999). In particular, the triggering and closure were completely overhauled (Rio et al., 2013) so that both the CP scheme (Grandpeix & Lafore, 2010) and the thermal plume scheme (Rio & Hourdin, 2008) control triggering and closure. Therefore, convection is tightly governed by subgrid, subcloud layer processes (Hourdin et al., 2020; Mapes, 1997). For the other parameterizations, in WRF we used the Rapid Radiative Transfer Model for GCMs longwave and shortwave radiation schemes (Iacono et al., 2008), the WSM6 microphysics scheme (Hong & Lim, 2006), the Yonsei University PBL scheme (Hong et al., 2006) which also computes the vertical diffusion due to turbulence, and the revised MM5 surface layer scheme based on Monin-Obukhov theory for surface fluxes computations (Jiménez et al., 2012). In the LMDZ runs, the radiation scheme is from an older European Centre for Medium-Range Weather Forecasts model (Morcrette, 1991). Boundary layer turbulence is handled by a prognostic turbulent kinetic energy diffusion scheme based on Yamada (1983) as well as by the mass flux thermal plume model. LMDZ also includes a large-scale condensation-precipitation-evaporation scheme and a gravity wave parameterization (Hourdin et al., 2013, 2020). In WRF, diurnal cycles were removed by setting the solar constant to 544 W m^{-2} and a fixed solar zenith angle of 37° to simulate equatorial conditions. In LMDZ, the diurnal cycle of

radiation was also removed. The simulations were run for 1,000 days in WRF and 60 days in LMDZ, thereafter two types of perturbations were applied, described in Sections 2.3 and 2.4. We note that the significantly longer simulation time for WRF is due to the disparate length of time taken by the different convection schemes to reach equilibrium (between 100 and 500 days). To be on the safe side we hence run the model for 1,000 days.

2.2. UW-*org* and LMDZ Cold Pool Schemes

In the UW-*org* scheme, the *org* variable can have several effects on convection (see Figure 1 in MN11). We focused on two of them: entrainment rate and closure. The fractional entrainment (ϵ) and detrainment (δ) rates per unit height in this scheme are given by

$$\epsilon = \epsilon_o \chi_c^2, \tag{2}$$

$$\delta = \epsilon_o (1 - \chi_c)^2, \tag{3}$$

where χ_c is the critical mixing fraction of environmental air in the parcels depending on height (see Equation B1 in Bretherton, McCaa, & Grenier, 2004), ϵ_o (m^{-1}) is the fractional mixing rate and is inversely proportional to height following a common formulation in literature (de Roode et al., 2000; Holloway & Neelin, 2009; Siebesma et al., 2007), that is, $\epsilon_o = k/z$. For the first plume k is an empirical constant (k_1) and set to a large value ($k_1 = 14$) following the original UW shallow scheme (entrainment rates are usually larger in shallow convection schemes), while k for the second plume (k_2) undergoes *org* modification following the equation

$$k_2 = \frac{k_1}{1 + org \cdot org2rkm}, \tag{4}$$

where *org2rkm* is a unitless parameter, and *org* is defined in Equation 1. Simply put, the *org*-modulated entrainment rate impacts convection development via its changing effect over time: during early stages when rain rates are small (small *org* values, as rain evaporation is a source of *org*) big entrainment rates suppress convection and promote the development of large-scale variability (i.e., organization), while in later stages large rain rates (large *org* values) lead to reduced entrainment rates that encourage deeper convection that stabilizes the column.

The second *org* effect we explored is its impact on cloud-base mass flux (CBMF; i.e., closure), which is computed as

$$M_b = M_{b,1}(1 + org \cdot org2cbmf), \tag{5}$$

where *org2cbmf* is a unitless parameter, $M_{b,1}$ is the CBMF of the first plume (given by Equation A3 in Park & Bretherton, 2009). The sinking of chilled air from downdrafts can potentially trigger convection by influencing plume base vertical velocity. This has the effect of larger CBMFs on rainy days when *org* values are big and the plumes have a higher probability of overcoming convective inhibition (CIN) and attaining their level of free convection (the scheme's closure is based on CIN).

We tested a few *org* configurations by changing and combining the *org2rkm* and *org2cbmf* parameters. For brevity, we refer to the cases where only *org2rkm* was changed as "WRF-RKM" and those where both *org2rkm* and *org2cbmf* were changed as "WRF-RKMCBMF."

For the LMDZ CP scheme, the version used here represents a population of circular, identical cold pools of radius *r*. The cold pools are assumed to have a fixed number density D_{CP} (m^{-2}) which sets how many cold pools there are per unit area. Hence, they occupy a relative surface area

$$\sigma_{CP} = D_{CP}\pi r^2. \tag{6}$$

Cold pools can expand horizontally at a horizontal spread speed *C* following a simple geometrical relation:

$$\frac{\partial \sigma_{CP}}{\partial t} = 2C\sqrt{\pi D_{CP}\sigma_{CP}}, \tag{7}$$

although their expansion is capped as soon as they reach the maximum allowed relative surface area $\sigma_{CP,\max} = 0.4$.

Cold pools are characterized by the vertical profile of their potential temperature and humidity differences with the external air around them (θ' and q'). Since they are denser than their environment, cold pools have a downward

Table 1
Models and Experimental Cases in This Study

Model	Convection scheme	Case name	*org* parameters	Description
WRF	Standard WRF convection schemes	ZM, KF, NT, NSAS, BMJ	–	Conventional convection schemes in WRF
	UW-*org*	rkm0	org2rkm = 0	Two identical plumes, no *org* effects (memory) in second plume
		rkm10	org2rkm = 10	Second plume has *org* effects
		rkm20	org2rkm = 20	
		rkm40	org2rkm = 40	
		rkm10cbmf10	org2rkm = 10, org2cbmf = 10	
		rkm20cbmf10	org2rkm = 20, org2cbmf = 10	
		rkm40cbmf10	org2rkm = 40, org2cbmf = 10	
LMDZ	Cold pool + Modified Emanuel/ALP/ALE schemes	LMDZ-CP	–	LMDZ5B+ version, settings for tropical ocean

vertical velocity which is transformed into horizontal spread speed C which can then be converted into upward motion at the cold pool edge. The total energy available for this mechanical process is the integrated negative buoyancy in cold pools, called Available Lifting Energy (ALE):

$$ALE = -g \int_0^{h_{CP}} \frac{\delta \theta_v}{\bar{\theta}_v} \, dz, \tag{8}$$

where h_{CP} is the cold pool height, g gravity, θ_v virtual potential temperature, and $\bar{\theta}_v$ denotes the grid cell mean θ_v. Deep convection is triggered when ALE > |CIN| (ALE being the largest between the ALEs provided by cold pools and PBL thermals), that is, when PBL processes are strong enough to erode boundary layer stability. In particular, PBL thermals may trigger convection only if a stochastic triggering condition is fulfilled (Rochetin, Couvreux, et al., 2014; Rochetin, Grandpeix, et al., 2014).

The experimental cases in this study are listed in Table 1.

2.3. FixMacro Experiment

We first consider the "strong-nudging" experiment by CS21, where the macrostate was fixed to its RCE mean. In the WRF CRM of CS21 (a non-aggregated setup), this was achieved by applying a tendency term for potential temperature (θ), water vapor mixing ratio (q) and horizontal winds (u, v) uniformly in (x, y) at each model level, proportional to the difference between the horizontal mean field and a target profile, with a short nudging time scale of 40 s (see Equation 1 in CS21). The idea is that if the diagnostic assumption used in convection schemes were true—using CS21's notation, convective activity C were related to the macrostate ξ via a function (f) : $C(\mathbf{x}, t) = f[\xi(\mathbf{x}, t)]$—convective activity would remain unchanged while the macrostate is held fixed. In the presence of microstate memory, however, in addition to its dependence on the large-scale environment convection also remembers its own history. That is, (f) : $C(\mathbf{x}, t) = f[\xi(\mathbf{x}, t), C(\mathbf{x}, t - 1)]$, and convection will not remain unchanged but will evolve in time under the influence of the macrostate rather than being determined by it instantaneously. Fixing the macrostate hence serves as a simple and direct test for microstate memory.

In the WRF SCM we emulate this experiment of CS21 via our fixed-macrostate ("FixMacro") experiment. Instead of nudging as in CS21, however, we restarted the SCM from its control macrostate and call the convection schemes with identical input profiles of thermodynamic and wind fields at every time step. This FixMacro approach achieved the desired result more directly and was feasible in the WRF SCM due to the model's modular design. We modified the code of the convection schemes such that at every time step the prognostic variables received by the schemes were overwritten with the values from specific target profiles. An ensemble of 20 FixMacro experiments was run, each with a target profile taken from a 20-day average of the unperturbed control run at a different time interval. We also attempted these SCM experiments using the CRM strong-nudging method, which yielded similar results (not shown).
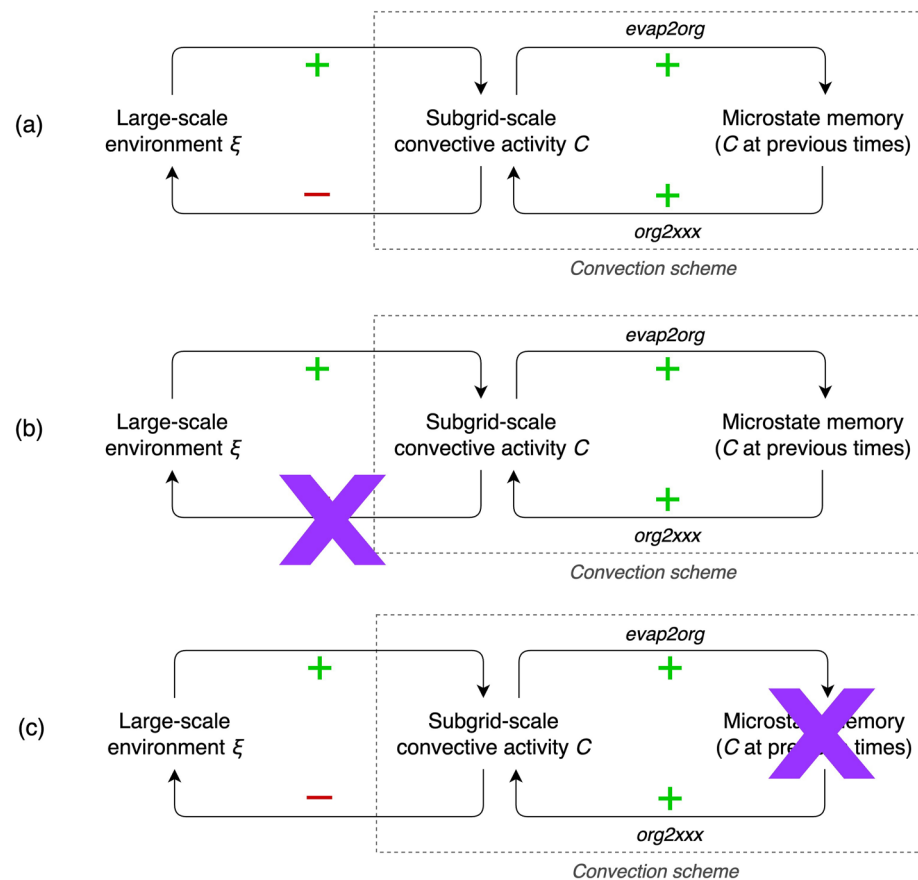
Figure 1. Diagram of the macro- and microstate feedbacks for the (a) control, (b) FixMacro (holding macrostate constant at every time step), and (c) HomoMicro (setting memory variable to zero at one time step) experiments. Green positive and red negative symbols indicate, respectively, positive and negative feedbacks on convection C or on environmental instability ξ favoring C. Italicized words are parameters in the UW-*org* scheme (see text for description).

Note that this FixMacro part of the experiment was only conducted in the WRF and not LMDZ SCM because in LMDZ it was technically challenging to directly fix the prognostic variables received by the convection scheme specifically.

2.4. HomoMicro Experiment

We next consider the "HomoMicro" experiment based on C19, where the WRF CRM control runs were restarted from equilibrated RCE states (for non-aggregated, windshear-aggregated, and self-aggregated setups) and subsets of prognostic variables (T, q, u, v and others) were horizontally homogenized to their domain-mean values at restart. This keeps the macrostate unchanged while essentially wiping out their microstate structures or memory. The equivalent with parameterized physics would be to set internal prognostic or "memory" variables to some reference value (e.g., zero). In the UW-*org* scheme there is a single such variable *org*, while in the LMDZ CP scheme there are prognostic cold pool temperature and moisture anomalies (T' and q'). For WRF UW-*org* we ran one test setting *org* to zero, while with LMDZ we ran three tests, zeroing either the T', the q', or both. An ensemble of 20 HomoMicro simulations was conducted for each test, as for FixMacro. Note that this part of the study cannot be conducted for the five standard WRF convection schemes, as they do not contain a microstate memory variable, so they implicitly predict no change after homogenization. A diagram of the control, FixMacro and HomoMicro experiments is shown in Figure 1.
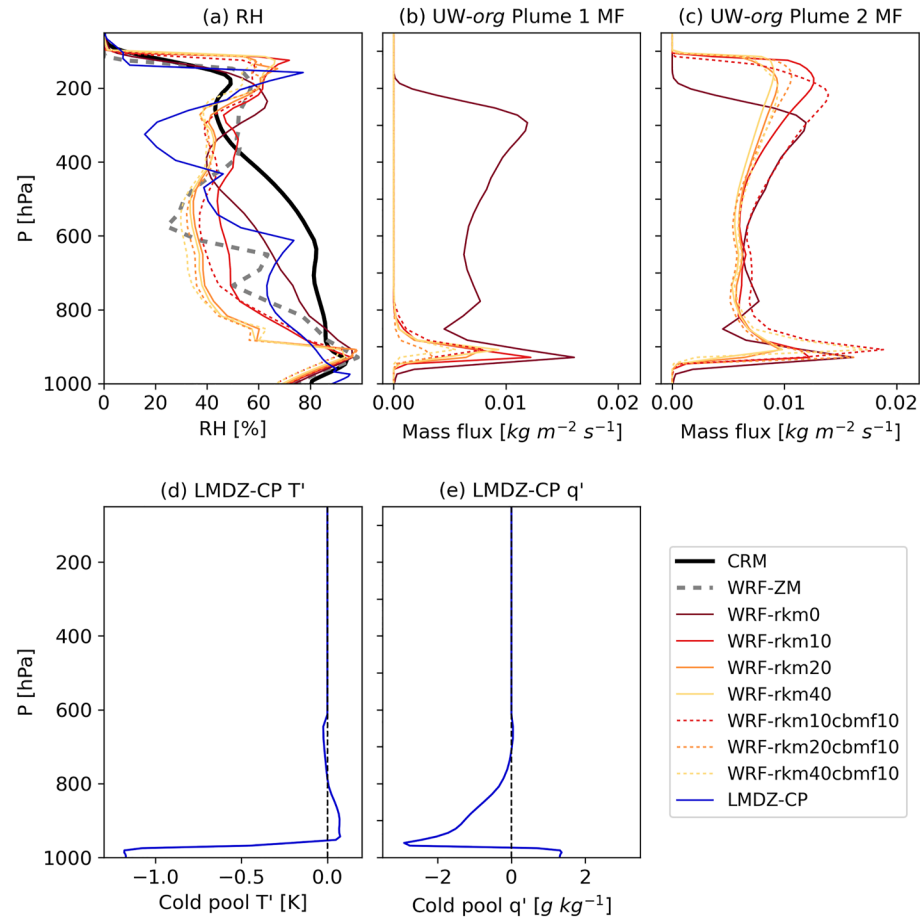
Figure 2. Radiative-convective equilibrium steady state profiles of (a) relative humidity (RH) for the cloud-resolving model (CRM) and various single-column model (SCM) configurations (for WRF SCM, only the Zhang-McFarlane and UW-*org* schemes are shown), (b, c) mass fluxes of the first and second plumes of the various UW-*org* configurations for the WRF SCM, and (d, e) temperature and moisture anomalies inside cold pools for the LMDZ SCM.

3. Results and Discussion

3.1. RCE Mean State

To illustrate the main features of the various model configurations we show the RCE mean state profiles of the relative humidity (RH) of the CRM (non-aggregated case), LMDZ and WRF SCM (for the standard convection schemes only ZM is shown as the other schemes have been presented in Hwong et al. (2021)), updraft mass flux of each plume in the WRF UW-*org* SCM, and the cold pool temperature and moisture anomalies of the LMDZ SCM, in Figure 2. There is a spread of around 20% of near-surface RH among the SCMs (panel a), with LMDZ displaying the moistest low-level profile (around 90%). This spread is comparable to that seen in previous SCM intercomparisons (e.g., Hwong et al., 2021; Wing et al., 2020). Hwong et al. (2021) found a difference of around 30% at near-surface levels even with constrained surface fluxes and a prescribed radiative profile in all models, and attributed this spread to the different parameterizations (primarily convection schemes) used in the SCMs. The CRM near-surface RH profile lies close to the middle of the SCM spread while in the free troposphere it is significantly moister, presumably due to the non-aggregated RCE state of the case shown here (details of the CRM mean state are described in C19 and CS21). For the UW-*org* cases, configurations with smaller entrainment rates (larger *org2rkm* values) display a drier free tropospheric mean state, suggesting more precipitation-efficient convection and hence stronger net drying. The UW-*org* cases also do not display the sharp changes (kinks) around the freezing level (~600 hPa) frequently seen in convection schemes (Hwong et al., 2021), although this is unlikely to be due to the addition of memory effect via *org*, as evidenced by the smooth RH free tropospheric profile of the rkm0 case, which does not contain *org* effects. We further note that the spread of RH in the

troposphere here is smaller than reported in previous model intercomparisons, which indicates that—although it does have significant impact—changing the *org* settings is less impactful than changing convection schemes.

The mass flux profiles of the two plumes in the UW-*org* scheme cases are shown in panels b and c. For the rkm0 case (two identical plumes and no *org* effect) the two plumes display the same mass flux profiles, while for the other cases a "division of labor" mechanism develops between the plumes: the second plume, with its reduced entrainment due to the *org2rkm* effect, takes up the role of deep convection (deeper than in rkm0) while the first plume, with its high entrainment rate as determined by the default UW shallow convection scheme parameters, assumes the function of shallow convection (confined below 850 hPa). Further, the addition of *org* effects in the closure (via *org2cbmf*; dashed lines in Figure 2) manifests itself in the larger mass flux of the second plume around the cloud-base.

The cold pool temperature (T') and moisture (q') anomaly profiles of LMDZ-CP are shown in panels d and e. The profiles show a cold and moist anomaly at the surface levels, illustrating the effect of cold pools on the thermo-dynamic microstate of the model. Colder, drier, and deeper cold pools are more powerful to generate convection as their negatively buoyant air displaces the surface air, which is then forced to rise, providing upward mass flux for triggering (Equation 8) and closure. The cold pools in this particular RCE configuration are fairly shallow and not very cold, but enough to have some influence on future convection. In particular, cold pools in this control simulation are always dominant over thermals to trigger convection, because the ALE provided by cold pools is always one order of magnitude larger than the ALE provided by thermals. Stronger updrafts and downdrafts both create a more different thermodynamic profile between cold pools and their environment (larger T' and q'). Therefore, the stronger the unsaturated downdrafts given by the convection scheme, the colder the cold pools. And likewise, the stronger the updrafts, the colder the cold pools.

3.2. Response to Fixed Macrostate Perturbation

Figure 3 shows responses of the CRM and WRF SCM to the FixMacro experiment, where the macrostate (large-scale environment) was held fixed to the RCE state. We first briefly summarize the CRM results, which are described in detail in CS21. Around half of the ensemble members (four out of nine) show exponential precip-itation growth to unphysical values, an example of which is shown in Figure 3, while for the remaining members precipitation decays to zero. CS21 found the trajectory of precipitation (growth or decay) depends on the target profile: members exhibiting growth behavior generally have higher convective available potential energy (CAPE) values compared to the decaying members. The authors referred to this state of the model as an "unstable equilib-rium in a thermodynamically fixed mean environment." By restraining the macrostate—thus preventing it from freely evolving—we are essentially overriding the natural negative feedback loop between the large-scale envi-ronment and subgrid-scale activities (see Figure 1b). Under normal non-nudged circumstances, instability caused by the large-scale environment (e.g., water vapor or CAPE) would be rapidly eliminated by convective activity *C* (e.g., convective heating and drying), hence maintaining a state of balance between the macro- and microstates. Without this restoring branch in the system (red negative symbol in Figure 1), an unopposed positive feed-back loop established itself: a macrostate conducive (unfavorable) to convection results in increased (decreased) precipitation, boosting (weakening) microstate memory, which in turn enhances (reduces) precipitation. Cold pools, for example, are a well-known source of microstate memory that are aided by the evaporation of rain and aid convection themselves (Schlemmer & Hohenegger, 2016; Tompkins, 2001; Zuidema et al., 2017). Further, CS21 also found low-level microstate structures (standard deviation of temperature and moisture at 2 m) to be the first variables to change during the initial development of instability. These findings collectively suggest that boundary layer inhomogeneities are the primary source of microstate memory.

For the WRF SCMs, precipitation remains constant as expected for the standard convection schemes and rkm0 when the macrostate is fixed (panel a), illustrative of the diagnostic assumptions in these cases, that is, absence of microstate memory. As the five standard schemes all behave the same way, we only show the results of the ZM scheme here. For the cases with *org* effects, precipitation rates exhibit an initial growth stage (between 2 and 10 hr after FixMacro started), before stabilizing latest by around half a day. Similar to the CRM, either growth or decay in precipitation rates was observed amongst the ensemble members, with a smaller proportion showing decay (hence the overall growth shown in Figure 3). Precipitation and the *org* variable appear to be monotonically related: precipitation grows amongst members where *org* increases, and decays where *org* decreases. However, there are marked differences between the response trajectory of the *org* cases and the CRM. Using rkm10 as an
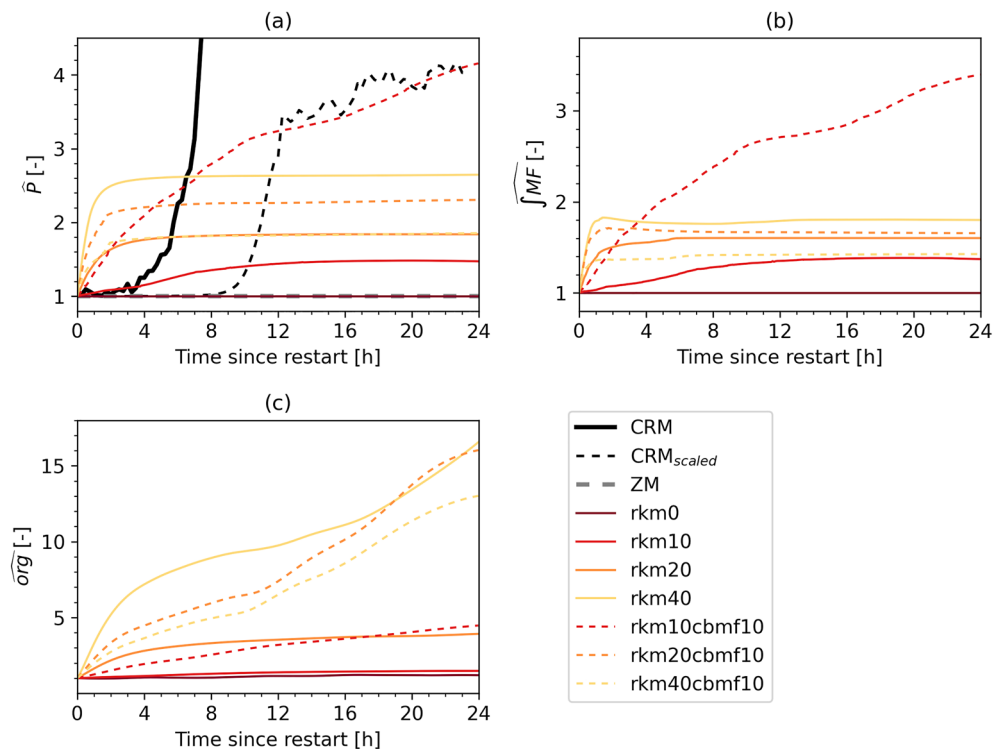
Figure 3. The FixMacro responses of normalized (a) precipitation of the cloud-resolving model (CRM), WRF-ZM and WRF UW-*org* cases, (b) integrated updraft mass flux and (c) *org* for the WRF UW-*org* cases. All responses are normalized by their respective RCE values when FixMacro begins. In panel (a), the normalized response of one of the CRM ensemble members (growing to ~3,000 mm day^{-1} from an RCE value of ~4 mm day^{-1}) is shown in thick black line and in dashed black line the same response scaled to the maximum range of the single-column models (SCMs). For the SCMs the final responses are obtained by averaging over all ensemble members. The RCE values are ~4 mm day^{-1} for P, ~0.3 kg m^{-1} s^{-1} for ∫MF and ~0.1 for *org*. The CRM response is reproduced from CS21. ©American Meteorological Society. Used with permission.

example, its response initially closely tracks that of the CRM, but starts to diverge from it by around 4 hr. While the CRM's growth accelerates exponentially, rkm10's growth appears to slow down and eventually stabilizes. We will further explore this discrepant response between the CRM and UW-*org* scheme in Section 3.3.

For the UW-*org* cases where *org* affects entrainment only (WRF-RKM), we found smaller entrainment rates (larger *org2rkm*) to be associated with more rapid precipitation-rate growth. This can be explained by stronger convection resulting from reduced mixing with environmental air, rendering a quicker feedback on the precipitation rate. The eventual departure from RCE also appears to increase with smaller entrainment rate. However, these trends are not consistently observed for the WRF-RKMCBMF cases: the precipitation rate of rkm40cbmf10 unexpectedly grows slower than rkm20cbmf10. This suggests that additionally including memory in the scheme's closure could have ambiguous effect, as multiple feedbacks come into play. For the corresponding cases where *org* also affects the closure (e.g., rkm10 vs. rkm10cbmf10; same-colored solid vs. dashed lines in Figure 3), faster initial precipitation growth rates and larger eventual departures from RCE were observed for the rkm10 and rkm20 cases, indicating that making the scheme's closure prognostic via dependence on *org* could act to enhance convection, thereby speeding up its reaction time.

We show in Figure 3 two additional variables that are useful to understand the precipitation response: integrated updraft mass flux (panel b) and *org* (panel c). The growth shape of the integrated updraft mass flux bears strong qualitative resemblance to that of precipitation (panel a), which is expected given the way the scheme diagnoses precipitation: updraft condensates exceeding a critical mixing ratio (1 g kg^{-1}) are expelled as precipitation (Bretherton, McCaa, & Grenier, 2004). As is common in mass flux schemes, the mass flux profile is used to compute all thermodynamic variables, including the precipitating condensates. Thus, precipitation is roughly proportional to the integral of mass flux over the convecting layer. For *org*, its growing response is emblematic of the microstate memory effect: *org* remembers its previous state and grows when precipitation

grows, since rain evaporation is a source of *org*. As mentioned, there appears to be a monotonic relationship between *org* and precipitation, at least in the initial growth stages. Given the fixed large-scale environment, this suggests that *org* (representing microstate memory) is chiefly responsible for the precipitation growth, and vice versa.

3.3. Why Does the UW-*org* Scheme Respond Differently to the CRM?

The initial exponential growth or decay of the CRM FixMacro responses presented in Section 3.2 can be explained using a PP model, as described in CS21, and which we briefly summarize here. For a detailed description of the PP model we refer readers to Section 3 of CS21. The three key equations of the PP model are:

$$\frac{\partial R}{\partial t} = E_0 - P, \tag{9}$$

$$\frac{\partial V}{\partial t} = \alpha_{vp}P - \alpha_{damp}V, \tag{10}$$

$$P = \alpha_p RV, \tag{11}$$

where R represents aspects of the macrostate environment that are conducive to convection but are also consumed by it (e.g., CAPE or water vapor), V represents features of microstate convective structures that stimulate convection and are stimulated by it (convective memory), E_0 is the source of R, P is precipitation, and α_{damp}, α_{vp}, and α_p are the damping rate of V, sensitivity coefficient of V to P and of P to the other variables, respectively. Under FixMacro conditions, Equation 9 equals to zero. Substituting Equation 11 into Equation 10 and fixing R to a constant R_0 (hereafter a zero subscript denotes the target FixMacro fixing values), combined with one of the steady state (RCE) solutions $R_{rce} = \frac{\alpha_{damp}}{\alpha_{vp}\alpha_p}$ (see Equations 5–7 of CS21), we get

$$\frac{\partial V}{\partial t} = \alpha_{vp}\alpha_p(R_0 - R_{rce})V, \tag{12}$$

which predicts an exponential growth (if $R_o > R_{rce}$) or decay (if $R_o < R_{rce}$) of V (and P, since they are linearly related when R is fixed). Expressed in terms of quantities normalized by their RCE values, Equation 12 can be reformulated as

$$\frac{\mathrm{d}\widehat{V}}{\mathrm{d}t} = \alpha_{damp}\left(a\,\widehat{V} - \widehat{V}\right), \tag{13}$$

where $\widehat{V} = V/V_{rce}$ and $a = R_0/R_{rce}$. Numerical integration of the PP model under FixMacro conditions indeed produces qualitatively the initial exponential growth of the CRM simulations (Figure 6 of CS21). Hence, by comparing the UW-*org* scheme to the PP model, we can gain useful insights that may shed light on the FixMacro behavior of the scheme when compared to the CRM.
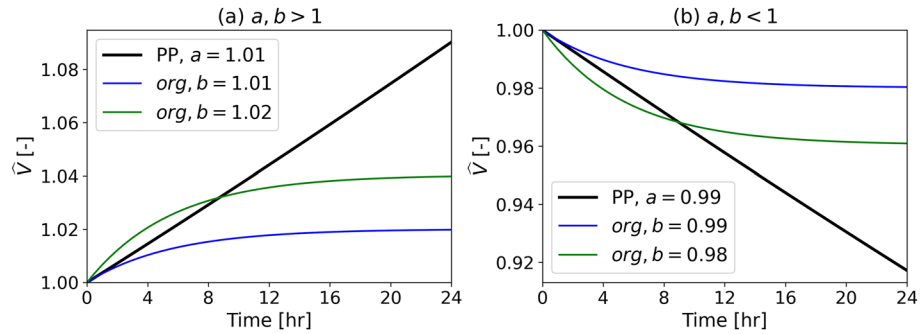
For the UW-*org* scheme, under FixMacro conditions we have observed a monotonic relationship between P and *org*, as presented in Section 3.2. For simplicity, and motivated by findings of previous studies (e.g., Kirsch et al., 2021; Kruse et al., 2022), we assume a linear approximation:

$$P = \beta\,org, \tag{14}$$

where β is the proportionality factor. Equation 1, describing the UW-*org* scheme, is roughly equivalent to Equation 10 of the PP model, with $V \equiv org$, $\alpha_{damp} \equiv 1/\tau_{org}$, and $\alpha_{vp}P \equiv evap2org \cdot E$, where E is the mass-weighted vertical integral of rain evaporation rate and is proportional to $(1 - RH)$ multiplied by the square root of P (Equation A8 in Park & Bretherton, 2009). Replacing *org* with V and reformulated in terms of quantities normalized by their RCE values to ease comparison with the PP model, Equation 1 can be simplified as

$$\frac{\mathrm{d}\widehat{V}}{\mathrm{d}t} = \alpha_{damp}\left(b\sqrt{\widehat{V}} - \widehat{V}\right), \tag{15}$$

where $\alpha_{damp} = 1/\tau_{org}$ and $b = \frac{1-\overline{RH_0}}{1-\overline{RH_{rce}}}$, with overbar indicating vertical mean values (see Appendix A for a detailed derivation of Equation 15).

Figure 4. Timeseries of memory variable $\widehat{V}$ under FixMacro conditions predicted by numerical integration of Equation 13 of the predator-prey (PP) model and Equation 15 of the UW-*org* scheme for the (a) growth and (b) decay cases. Note that the PP curve displays an exponential trajectory similar to the cloud-resolving model response shown in Figure 3 when integrated over a longer period of time, even though it appears linear within the 24 hr shown here.

Equations 13 and 15 are equivalent versions of the prognostic equation for the memory variable V in the PP model and UW-*org* scheme under FixMacro conditions. Applying a damping rate α_{damp} of 1×10^{-4} s^{-1} the timeseries of $\widehat{V}$ predicted by numerical integration of the two equations for the growth ($a, b > 1$) and decay ($a, b < 1$) cases are shown in Figure 4. The results bear strong qualitative resemblance to the simulated P responses presented in Section 3.2 (noting that the timeseries of P would be qualitatively similar to *org* or V given the assumption of their linear relationship). The impact of a small mismatch between the target FixMacro and RCE values is initially the same: for $a = b$, the P responses predicted by the PP model and the UW-*org* scheme initially closely follow each. Their behavior begins to depart only when P has changed significantly. In the PP model, $\frac{dP}{dt}$ is linearly related to P, producing exponential growth, and no value of P can restore the balance between the growth and decay terms on the RHS of Equation 13 if $a > 1$ (or $a < 1$ for the decay case). This reproduces the exponential growth (or decay) behavior observed in the CRM. By contrast, a negative feedback is built into the UW-*org* scheme because the growth term (first term on the RHS of Equation 15) increases more weakly with P than the damping term (second term on the RHS of Equation 15), which eventually brings the system toward a stable equilibrium. Note that this behavior is valid given any sub-quadratic function $P(org)$. In other words if $P = \beta \, org^{\lambda}$, then as long as $\lambda < 2$, $\widehat{org}$ (and P) will eventually stagnate under FixMacro conditions, as the source term in Equation 1 will grow slower than the sink term. In our case, scatterplots of model outputs from the FixMacro experiments show that P is approximately linearly related to *org* (not shown), which supports our assumption of a linear relationship (Equation 14).

We further note that for the *org* growth (decay) case, the condition of $b > 1$ ($b < 1$) can only be met if the FixMacro target profile for RH is such that $\overline{RH}_0 < \overline{RH}_{rce}$ $\left(\overline{RH}_0 > \overline{RH}_{rce}\right)$. Indeed, we found these conditions to be true for the respective growing and decaying ensemble members (not shown). Additionally, the *org* cases with faster growth rates generally also have larger average b values (e.g., rkm10 vs. rkm20 in Figure 3), consistent with the results shown in Figure 4. We have also found that τ_{org} influences the growth and decay rates: when τ_{org} increases (decreases), *org* is consumed at a slower (faster) rate, which leads to stronger (weaker) memory and hence slower (faster) growth and decay rates (not shown).

Overall, our results provide strong evidence that, assuming a linear damping term, the CRM supports a linear (or superlinear) relationship between subgrid-scale structure growth rate and the current precipitation rate. Given a linear damping, any scheme that predicts a sublinear relationship would eventually stabilize under FixMacro conditions. The FixMacro perturbation described here can thus be applied as a simple test to probe the behavior of convection schemes and constrain core modeling assumptions. Nevertheless, several caveats must be noted. First, although our assumption that P is proportional to *org* only captures the leading order qualitative behavior and is not exactly quantitatively accurate, our goal is to probe whether the trajectory of P under FixMacro conditions can be understood from the scheme's structural assumptions. Our numerical results presented here, albeit idealized, can shed light into how the P responses can be explained by the scheme's governing equations. Second, by using the CRM as a benchmark, we have made the implicit assumption that the scheme's more stable response is somehow an erroneous behavior compared to the CRM's exponential growth. Whether this assumption is fair remains an open question. There are often sound operational reasons to put in checks and balances in a convection

scheme—however unrealistic or ad hoc though they may be—to prevent simulations from crashing in a GCM (as an exponential precipitation growth would be prone to do). Additionally, the absence of dynamical coupling in an SCM setup could potentially limit the validity of a full comparison to the CRM results, especially for memory that may emerge from feedback with large-scale circulations. However, here, (a) we isolate the memory at subgrid scales (microstate memory) and do not focus on the memory related to large-scale circulations (macrostate memory), (b) there is no significant organization (and hence minimal mesoscale circulations) in the CRM reference that we used, thus enabling a more direct comparison of memory behavior between the CRM and SCM in the FixMacro experiments. Despite these caveats, it is nonetheless useful to be able to verify that the scheme's FixMacro responses do indeed comply with its structural assumptions, and that its discrepant response to the CRM can thus be explained.

3.4. Response to Instantaneous Change in Microstate

Figure 5 shows the responses of the CRM and SCMs in the HomoMicro experiment described in Section 2.4, in which subgrid-scale variabilities at RCE were homogenized at one time step without changing the column/domain average. We show a selection of C19's CRM results in panel a. In most of these CRM cases, homogenization results in a drop to (close to) zero in precipitation rates, which then recover to their respective RCE values over a certain time period, defined here as t_{mem} (black dots in Figure 5). If convection were solely dependent on the macrostate, precipitation would recover almost instantly, as the homogenization step only affects the microstate. The time the system takes to recover (t_{mem}) is hence a measure of the strength of the microstate memory. In effect, the homogenization step removes the subgrid-scale structures that are conducive to convection, hence the system needs to "start from scratch" and wait for instability to build up again before precipitating. C19 found that memory is mostly stored in thermodynamic heterogeneities, rather than winds or hydrometeors. In particular, low-level water vapor variability is the dominant memory carrier. For simulations where convection is unorganized, homogenizing both T and q led to the longest recovery time (2.5 hr), followed by only T (2 hr) and q (1.5 hr) homogenization. In contrast to the other variables, homogenizing T leads to an initial increase in precipitation. C19 explained this by noting that the precipitating locations usually have cold pools and hence also a colder boundary layer. Homogenizing T therefore resulted in an increase in MSE in these locations (instead of a decrease as when only q or both T and q were homogenized), leading to an increase in precipitation. Further, convective organization leads to a drastic increase in memory, as seen in the significantly longer t_{mem}'s of the wind-shear organized (12 hr) and self-aggregated (>24 hr) cases where both thermodynamic quantities were homogenized.

In the SCMs, we mimicked the CRM HomoMicro perturbation by setting the memory variable(s) (*org* in the UW-*org* scheme in WRF, T' and/or q' in LMDZ-CP) to zero at one time step. For LMDZ-CP (panel b), HomoMicro led to an initial growth instead of reduction in precipitation for all three cases, with very similar t_{mem}'s of 1–2 hr, which are comparable to the CRM's unorganized cases. We think that the increase in precipitation of LMDZ-CP after HomoMicro is related to the fact that in all cases, the perturbation increases ALP, which directly controls convection intensity (closure). Interestingly, the ALE (triggering) provided by cold pools is successfully decreased by HomoMicro for about 10–15 min when T' or both T' and q' are set to zero. Likewise, the ALP provided by cold pools also decreases after HomoMicro for about 45 min for these two tests. However, it is the ALP provided by the PBL thermals that dramatically increases for 15 min after HomoMicro and causes precipitation to first increase. After rain increases, cold pools become colder, more powerful, and they partially maintain an additional supply of mass flux. In contrast to the diverse CRM responses to the three types of homogenization (T, q or Tq), LMDZ-CP displays similar behavior in all three. The CRM recovery time almost doubled when homogenizing both Tq compared to when only T or q was homogenized, while in LMDZ-CP t_{mem} when both Tq were homogenized is almost the same as when homogenizing only T. Analyses of the responses of cold pool properties (T', q' and cold pool surface area) also show that homogenizing Tq and T only led to almost identical behavior. Moreover, T homogenization has a clear impact on q', but q homogenization did not affect T'. These results suggest that memory is mainly carried by the temperature variable in the LMDZ-CP scheme (Colin, 2020), as opposed to a dominant moisture memory in the CRM.

For the UW-*org* cases with memory (panels c, d), the responses are strikingly similar to the CRM where both thermodynamic variables or only moisture were homogenized, with precipitation falling immediately almost to zero, then overshooting and finally returning to RCE. Although both schemes employ rain evaporation as the memory source, it appears that—in contrast to LMDZ-CP—the UW-*org* scheme contains a stronger moisture memory
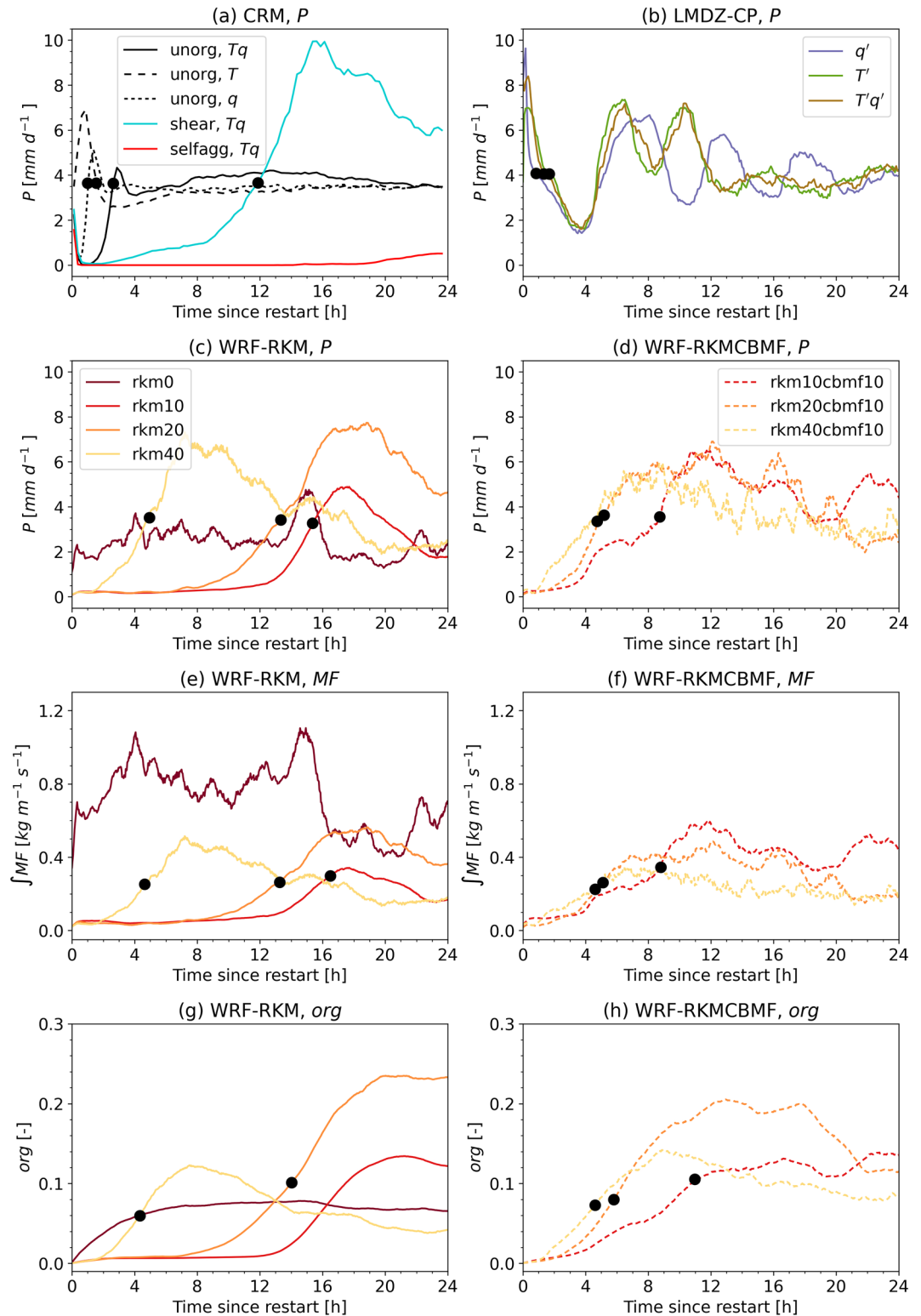
Figure 5. The HomoMicro ensemble-averaged responses of precipitation of the (a) cloud-resolving model (CRM), (b) LMDZ-CP, (c) WRF-RKM, and (d) WRF-RKMCBMF cases. The responses of the vertically integrated updraft mass flux and *org* of the (e, g) WRF-RKM and (f, h) WRF-RKMCBMF cases are also shown. Black dots indicate the times t_{mem} (*x* coordinates) when the responses first recover to the RCE values (*y* coordinates) in the respective control runs. Note that the *org* recovery time for rkm10 is ∼30 hr and hence not visible in panel (g). The CRM responses are reproduced from C19. ©American Meteorological Society. Used with permission.

effect, reminiscent of the CRM response. The responses are especially close to the wind-shear experiment in the CRM, which had an intermediate level of convective organization. Since *org* represents subgrid-scale variability that both promotes and is promoted by convection, setting its value to zero is akin to removing the self-enhancing effect of convection via its own memory (positive feedback), hence precipitation takes time to build up again (see Figure 1c). As expected, the rkm0 case (which does not contain memory) does not respond to the perturbation. Similar to the FixMacro results, we again found the time evolutions of the integrated mass flux (panels e, f) to be very similar to those of precipitation. There is also a strong resemblance between the recovery of *org* and precipitation, albeit to a lesser extent for rkm10, which takes a longer time (∼30 hr) to recover to its RCE value. Additionally, longer recovery times here appear to correspond to slower precipitation growth in the FixMacro experiment for the WRF-RKM cases (but this observation does not consistently apply for the WRF-RKMCBMF cases as noted in Section 3.2). For instance, rkm10 displays the longest recovery time here and the slowest growth in the FixMacro experiment. This is also true for corresponding WRF-RKM and WRF-RKMCBMF cases: cases where *org* also affects CBMF evolve more rapidly than their WRF-RKM counterparts in FixMacro and also recover more quickly here. This shows that both experiments have managed to capture similar aspects of memory, albeit via different perturbation methods.

Given the similarity between the responses and recovery times of *org* and precipitation described in this section and in the FixMacro experiment, it is reasonable to assume that *org* contains information about convective memory. *Org* influences entrainment rate and CBMF via Equations 4 and 5, which results in the different recovery times between the UW-*org* cases. We explore the *org* variable further in Section 3.5.

3.5. Convective Memory and *org*

The HomoMicro experiment revealed different t_{mem}'s between the UW-*org* cases. An important question then is the relationship between the *org* variable and the recovery times: if *org* adequately represents the effects of subgrid-scale heterogeneity, or convective organization, in principle it would be related to t_{mem}. Here, we explore the *org* variable and its relationship to convective memory. To improve statistical confidence, we conducted eight additional experiments with *org2rkm* = 5, 15, 40, 50 and additionally paired them with *org2cbmf* = 10, resulting in a total of 14 simulations for our analyses (excluding rkm0 as it does not contain memory). Additionally, to account for the possibility that setting *org* to zero may represent disparate effects for cases with different org_{rce} values (i.e., a configuration with larger org_{rce} value could display bigger t_{mem} simply because of the stronger perturbation incurred when *org* is set to zero), we conducted another set of experiments where we set *org* to a value equals to the respective RCE *org* values minus 0.05, representing the same absolute change for all configurations. We refer to this set of experiment as ORG_ABS and to the experiments where *org* is set to zero as ORG_ZERO.

Results are shown as scatterplots in Figure 6, where data from the final 300 days of the 1,000 days control simulations were used to derive the mean org_{rce} values (results are not sensitive to the averaging period). As some results contain outliers, in addition to Pearson correlation coefficient (r_p) we have also computed the Spearman's rank correlation coefficient (r_s), which is less sensitive to outliers. For ORG_ZERO, we found a very high correlation between t_{mem} and the mean values of org_{rce} (panel a). A high negative correlation (panel c) was also found between t_{mem} and the initial $d(\widehat{org})/dt$ immediately after HomoMicro was applied (where $\widehat{org} = org/org_{rce}$ as described in Section 3.3), indicating that a slower *org* recovery rate is associated with larger t_{mem}. For ORG_ABS, the strong association between t_{mem} and org_{rce} discovered for ORG_ZERO disappears (panel b), but a strong correlation remains between t_{mem} and the *org* growth rate (panel d). Note that removing the outlier (rkm10) from ORG_ABS does not significantly affect the results (correlations when rkm10 is omitted: $r_p = 0.4$, $r_s = 0.31$ for panel b; $r_p = -0.71$, $r_s = -0.78$ for panel d). With the exception of rkm10, the t_{mem}'s for the ORG_ABS cases are significantly more similar to each other (they are closer to each other in panels b and d) compared to the ORG_ZERO cases, pointing to the possibility that the highly linear relationship between t_{mem} and org_{rce} found for ORG_ZERO could be due to the more vigorous perturbation the homogenization step has when there is more *org* to be homogenized, which leads to longer recovery times.

Overall, the robustness of the results between panels c and d suggests that it is not the absolute value of *org* but its rate of change that encodes information about the memory strength of a system (before perturbation, it is the same RCE system in c and d, so it should have the same memory). Further evidence for this can be seen in the initial negative growth rates of a few configurations with the strongest memory (longest t_{mem}'s) in the ORG_ABS
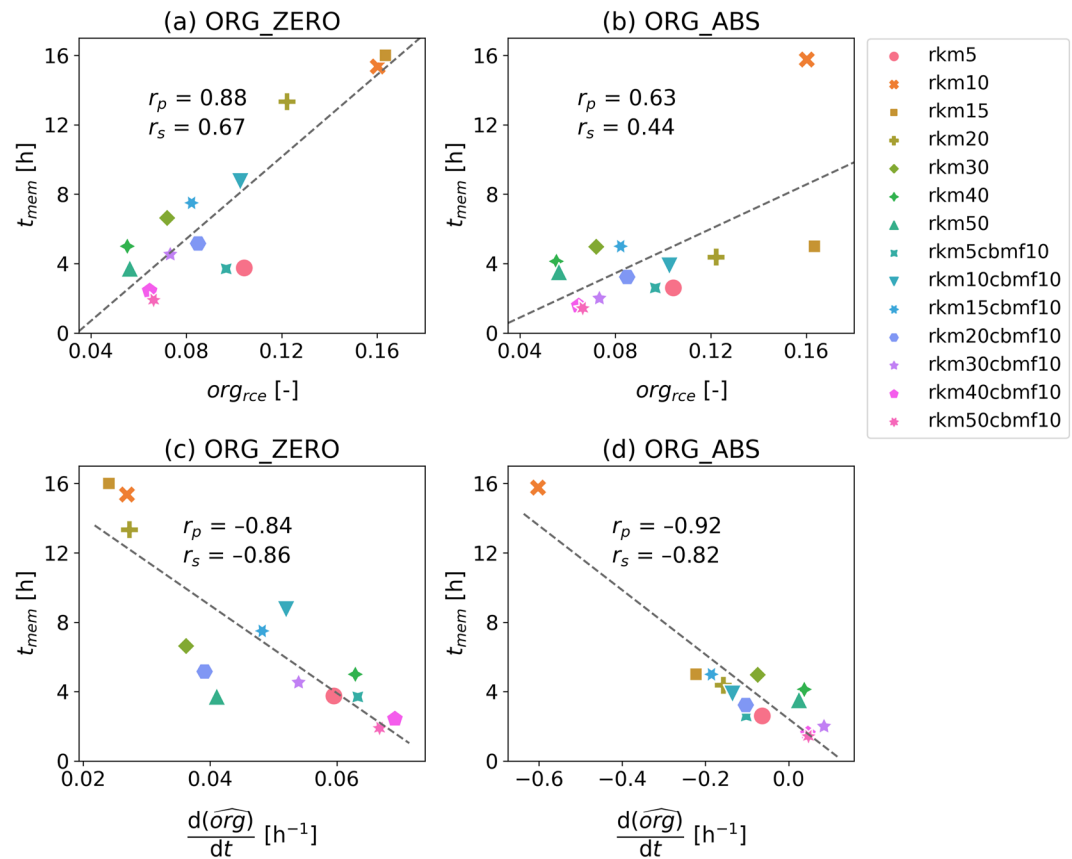
Figure 6. Scatterplots of t_{mem} versus the (a) mean org values at RCE for the ORG_ZERO experiment, where org is set to zero, (b) same as panel (a) but for the ORG_ABS experiment, where org is set to the respective org_{rce} values minus 0.05, (c) $\widehat{org}$ growth rate over one time step after HomoMicro begins for ORG_ZERO, and (d) same as panel (c) but for ORG_ABS. The Pearson and Spearman's correlation coefficients are shown as r_p and r_s, respectively.

experiment (panel d), indicating that org continued to decrease (instead of immediately recovering as in other cases) after the instantaneous homogenization step because of its higher inertia in these cases.

We also observed from Figure 6a that smaller entrainment rates (larger $org2rkm$) are sometimes associated with smaller values of org_{rce} and hence smaller rain evaporation rates (as rain evaporation is the source of org). This is somewhat surprising, given that drier mean RH profiles are associated with smaller entrainment rates as described in Section 3.1 and rain evaporation should increase in a drier environment. Upon closer inspection of the timeseries of rain evaporation $E(t)$ and precipitation flux $p'(t)$, we found that the decrease in mean state (i.e., time-averaged) $\overline{E}$ with decreasing entrainment rates could be due to two reasons: (a) rain evaporation is only allowed below the lifting condensation level (LCL) in the scheme, and the RH profiles below the LCL are very similar amongst the UW-org cases, hence diminishing the contribution of RH to the differences in rain evaporation rates between the cases, and (b) the computation of rain evaporation at every time step involves the multiplication of $(1 - RH)$ by precipitation flux p' (Equation A1 in Appendix A). Simulation results revealed that $p'(t)$ is highly variable and its variance increases while its mean decreases with decreasing entrainment rates below the LCL (this can also be deduced from the smaller mass flux values for larger $org2rkm$ cases below the LCL as shown in Figure 2, as precipitation is diagnosed from the updraft mass flux in the scheme). This potentially results in the higher variance of $E(t)$ and lower steady-state $\overline{E}$ values for the cases with smaller entrainment rates.

4. Conclusions

The main objective of the present study is to evaluate the memory behavior of several configurations of the UW-org scheme as well as the LMDZ CP convection scheme, with memory being defined as the dependence

of convection on its own history given its current environment. As control (memory-less) cases we also tested five conventional convection schemes. We compare the responses of these schemes in a SCM setup to those of a CRM using two idealized RCE experiments. The CRM results are taken from previously published studies (Colin et al., 2019; Colin & Sherwood, 2021), and include two tests: FixMacro, where we hold the macrostate environment of convection fixed and observe the evolution of convection; and HomoMicro, where we reset subgrid prognostic variables to neutral values at one time and observe the subsequent evolution as they recover. These tests serve two purposes. As presented in the previous studies, they allow us to test the diagnostic assumption where convective activity is assumed to be instantaneously and solely determined by the macrostate. As newly implemented here, they further allow us to differentiate between different possible parameterizations of convective memory processes.

The picture that emerges from these experiments can be summarized into three main points. First, standard convection schemes that do not contain any internal prognostic variables and diagnose convective behavior from their environment behave very differently to the CRM in the FixMacro experiment. Precipitation (a proxy for convective activity) remains invariant in time, while in the CRM it grows or decays exponentially. This invariance reveals the diagnostic assumption used in these convection schemes: convection is slave to and only to the macrostate, hence when the large-scale environment is restrained, convective activity also remains unchanged. These results are unsurprising, but nonetheless serve as a clear and easy-to-understand demonstration of the memory (or rather, lack thereof) behavior of schemes that employ the diagnostic assumption. Since the time scales of growth or decay shown by the CRM are many hours, this failure of diagnostic schemes is likely to cause large discrepancies in transient convective behavior on subdaily time scales.

Second, the memory-capable UW-*org* and LMDZ-CP schemes partially, but do not fully, capture the behavior of the CRM under FixMacro and HomoMicro conditions. For the UW-*org* scheme, precipitation mimics the behavior of the CRM in that precipitation either grows or decays when its large-scale environment is fixed, indicating the effects of microstate memory. However, its growth trajectory departs from that of the CRM after a few hours, trending toward a stable equilibrium, while in the CRM precipitation continues to evolve exponentially. This behavior can be explained by the scheme's structural assumptions, in particular that the impact of precipitation on the subgrid state scales sublinearly with precipitation, while the CRM exhibits a linear (or superlinear) dependence between the two. When the microstate memory variables are set to zero instantaneously, the UW-*org* scheme behaves similarly to the CRM cases where both Tq or only q were homogenized: precipitation falls to zero and then recovers to its RCE state. The LMDZ-CP scheme, on the other hand, displays responses that mimic the CRM behavior when only T was homogenized: precipitation grows before falling back to its RCE value after a few oscillations. We found the rate of change in time of *org* to be correlated with memory strength in both the FixMacro and HomoMicro experiments, suggesting that *org* has captured crucial aspects of memory.

Third, different ways convection schemes parameterize memory clearly have an impact on their behavior. Again, this might seem trivial and unsurprising, but it is useful to be able to highlight these differences in a clear and convincing way. One important difference that was revealed here was the dominant type of memory represented by the schemes. Even though both schemes use rain evaporation as their memory source (with explicit dependence on RH, a thermodynamic variable), the LMDZ-CP scheme appears to emphasize temperature-stored memory while the UW-*org* scheme displays a prevailing moisture memory response that is more similar to the CRM's behavior. This intriguing disparity is no doubt a manifestation of the general conceptual difference between the schemes and the way they aim to represent memory through their governing equations. Perhaps the UW-*org* scheme's use of a prognostic *org* variable that mimics the behavior of the prey in the PP equations (akin to Colin and Sherwood (2021)) was better at reproducing the CRM's behavior. Of course, whether our results imply one scheme's definitive superiority over another cannot be ascertained based only on two simple idealized tests: the LMDZ-CP scheme may very well perform better in other (perhaps more realistic) tests, which we have not taken into account here. Nevertheless, our findings could perhaps inspire ideas about or guide the search for ways to investigate potential flaws in a scheme.

Our study has several limitations. We have relied on results from a single CRM (WRF) to provide "truth" for assessing the convection schemes. Findings could potentially differ with another CRM. Even in the WRF CRM we found varying results with different states of convective organization. We hence cannot rule out the possibility that other model configurations (e.g., domain size, horizontal resolution) could also influence the results presented here. The two experiments conducted are highly idealized and do not resemble anything that would

happen naturally in the atmosphere, and thus potentially may be unfair tests of parameterizations that might reveal deficiencies that do not matter in practice. We acknowledge that these experiments are indeed more akin to laboratory experiments and are not meant to be realistic. However, they serve the purpose of providing ways to understand the behavior of convection schemes (which is not at all a straightforward endeavor) in a simple framework that may offer useful insights on their complicated behavior in realistic scenarios. Under steady-state conditions we investigated here (RCE), the importance of the temporal dependence of convection on its own past state (i.e., the prognosticity of the memory variable) may not be as apparent compared to transient scenarios. Nonetheless, the memory time scales revealed in our experiments (~12 hr in the UW-*org* scheme) are very similar to that of the diurnal cycle as well as the moisture adjustment time scale observed over the tropical oceans (Bretherton, Peters, & Back, 2004), suggesting that our experiments have likely isolated issues related to the inability of some memory-less schemes in the correct simulation of diurnal cycles (Daleu et al., 2020; Harvey et al., 2022). Lastly, our SCM setup necessarily means that no insights about convective organization can be provided, which limits the interpretation of certain results. The connection between convective memory and organization, for example, cannot be verified. Nevertheless, 1D and 3D results have been found to be comparable (Hwong et al., 2022), suggesting there is a chance the findings of our study can be applied to improve temporal memory parameterization, which in turn could help improve the representation of spatial organization (Tobin et al., 2013). It is therefore a high priority to validate the results discussed here using a 3D setup.

Appendix A: Derivation of *org* Prognostic Equation

The source term of the *org* prognostic equation (Equation 1) is $evap2org \cdot E$, where E is the mass-weighted vertical integral of rain evaporation rate, given by the following equation (Equation A8 in Park & Bretherton, 2009):

$$E = \int_0^{LCL} (1 - \mathrm{RH})\sqrt{K_e^2 \; p'} \; \rho \; \mathrm{d}z, \tag{A1}$$

where RH, p' and ρ are the vertical profiles of RH, precipitation flux and air density, respectively, LCL is the lifting condensation level, and K_e is a constant and has the value of 0.2×10^{-5} [(kg m^{-2} s^{-1})$^{-1/2}$ s^{-1}] (Park & Bretherton, 2009). E and p' are in the units of kg m^{-2} s^{-1}. To enable a more numerically tractable formulation, we simplify Equation A1 to

$$E = K\left(1 - \overline{\mathrm{RH}}\right)\sqrt{P}, \tag{A2}$$

where P is surface precipitation (in units kg m^{-2} s^{-1}), $\overline{\mathrm{RH}}$ is the vertical mean of RH, and K is a constant (in units [kg m^{-2} s^{-1}]$^{1/2}$). Note that this simplified equation for E is valid within individual simulations, but should not be applied to compare between different UW-*org* cases using their steady-state values of $\overline{\mathrm{RH}}$ and $\overline{P}$.

Substituting Equation A2 in Equation 1 we get

$$\frac{\mathrm{d}(org)}{\mathrm{d}t} = evap2org \cdot K\left(1 - \overline{\mathrm{RH}}\right)\sqrt{P} - \frac{org}{\tau_{org}}, \tag{A3}$$

We have assumed a linear approximation for the relationship between P and *org* (i.e., $P = \beta org$), Equation A3 thus becomes

$$\frac{\mathrm{d}(org)}{\mathrm{d}t} = evap2org \cdot K\left(1 - \overline{\mathrm{RH}}\right)\sqrt{\beta \; org} - \frac{(org)}{\tau_{org}}, \tag{A4}$$

There are two steady state (RCE) solutions to the system $\left(\frac{\mathrm{d}(org)}{\mathrm{d}t} = 0\right)$, one of which is $org_{rce} = 0$, and the other one gives

$$\sqrt{org_{rce}} = \sqrt{\beta} \; evap2org \cdot K\tau_{org}\left(1 - \overline{\mathrm{RH}}_{rce}\right). \tag{A5}$$

Combining Equations A4 and A5 by substituting *evap2org* we get

$$\frac{\mathrm{d}(org)}{\mathrm{d}t} = \frac{org_{rce}}{\tau_{org}}\left[\left(\frac{1 - \overline{\mathrm{RH}}}{1 - \overline{\mathrm{RH}}_{rce}}\right)\sqrt{\frac{org}{org_{rce}}} - \frac{org}{org_{rce}}\right]. \tag{A6}$$

Under FixMacro conditions, Equation A6 can be formulated in terms of a normalized *org*, with $\widehat{org} = org/org_{rce}$, and a FixMacro profile, $\overline{RH}_0$

$$\frac{d\left(\widehat{org}\right)}{dt} = \frac{1}{\tau_{org}}\left(b\sqrt{\widehat{org}} - \widehat{org}\right),$$

(A7)

where $b = \frac{1-\overline{RH}_0}{1-\overline{RH}_{rce}}$. Substituting $\widehat{org}$ with the normalized memory variable $\hat{V}$ we get Equation 15. Numerical integration of Equation A7 shows that, for an initial value of $\widehat{org}_0 = 1$ (i.e., $org = org_{rce}$),

$$\begin{cases} \widehat{org} = 1, & \text{if } b = 1, \text{control case.} \\ \frac{d(\widehat{org})}{dt} > 0, & \text{if } b > 1, \text{FixMacro growth case.} \\ \frac{d(\widehat{org})}{dt} < 0, & \text{if } b < 1, \text{FixMacro decay case.} \end{cases}$$

(A8)

Data Availability Statement

The data, scripts and model source codes and files required to reproduce the results described in this manuscript are available at https://zenodo.org/record/8073523 (Hwong et al., 2023).

References

Arakawa, A., & Schubert, W. H. (1974). Interaction of a cumulus cloud ensemble with the large-scale environment, Part I. *Journal of the Atmospheric Sciences*, *31*(3), 674–701. https://doi.org/10.1175/1520-0469(1974)031<0674:ioacce>2.0.co;2

Bechtold, P., Köhler, M., Jung, T., Doblas-Reyes, F., Leutbecher, M., Rodwell, M. J., et al. (2008). Advances in simulating atmospheric variability with the ECMWF model: From synoptic to decadal time-scales. *Quarterly Journal of the Royal Meteorological Society*, *134*(634), 1337–1351. https://doi.org/10.1002/qj.289

Becker, T., Bretherton, C. S., Hohenegger, C., & Stevens, B. (2018). Estimating bulk entrainment with unaggregated and aggregated convection. *Geophysical Research Letters*, *45*(1), 455–462. https://doi.org/10.1002/2017gl076640

Bengtsson, L., Dias, J., Tulich, S., Gehne, M., & Bao, J.-W. (2021). A stochastic parameterization of organized tropical convection using cellular automata for global forecasts in NOAA'S Unified Forecast System. *Journal of Advances in Modeling Earth Systems*, *13*(1), e2020MS002260. https://doi.org/10.1029/2020ms002260

Bengtsson, L., Steinheimer, M., Bechtold, P., & Geleyn, J.-F. (2013). A stochastic parametrization for deep convection using cellular automata. *Quarterly Journal of the Royal Meteorological Society*, *139*(675), 1533–1543. https://doi.org/10.1002/qj.2108

Betts, A. (1986). A new convective adjustment scheme. Part I: Observational and theoretical basis. *Quarterly Journal of the Royal Meteorological Society*, *112*(473), 677–691. https://doi.org/10.1002/qj.49711247307

Betts, A., & Miller, M. (1986). A new convective adjustment scheme. Part II: Single column tests using GATE wave, BOMEX, ATEX and arctic air-mass data sets. *Quarterly Journal of the Royal Meteorological Society*, *112*(473), 693–709. https://doi.org/10.1002/qj.49711247308

Bretherton, C. S., McCaa, J. R., & Grenier, H. (2004). A new parameterization for shallow cumulus convection and its application to marine subtropical cloud-topped boundary layers. Part I: Description and 1D results. *Monthly Weather Review*, *132*(4), 864–882. https://doi.org/10.1175/1520-0493(2004)132<0864:anpfsc>2.0.co;2

Bretherton, C. S., Peters, M. E., & Back, L. E. (2004). Relationships between water vapor path and precipitation over the tropical oceans. *Journal of Climate*, *17*(7), 1517–1528. https://doi.org/10.1175/1520-0442(2004)017<1517:rbwvpa>2.0.co;2

Caseri, A. N., Santos, L. B. L., & Stephany, S. (2022). A convolutional recurrent neural network for strong convective rainfall nowcasting using weather radar data in southeastern Brazil. *Artificial Intelligence in Geosciences*, *3*, 8–13. https://doi.org/10.1016/j.aiig.2022.06.001

Cohen, B. G., & Craig, G. C. (2004). The response time of a convective cloud ensemble to a change in forcing. *Quarterly Journal of the Royal Meteorological Society*, *130*(598), 933–944. https://doi.org/10.1256/qj.02.218

Colin, M. (2020). Convective memory, and the role of cold pools (Doctoral dissertation) (p. 356). UNSW Sydney. Retrieved from http://handle.unsw.edu.au/1959.4/70757

Colin, M., Sherwood, S., Geoffroy, O., Bony, S., & Fuchs, D. (2019). Identifying the sources of convective memory in cloud-resolving simulations. *Journal of the Atmospheric Sciences*, *76*(3), 947–962. https://doi.org/10.1175/jas-d-18-0036.1

Colin, M., & Sherwood, S. C. (2021). Atmospheric convection as an unstable predator–prey process with memory. *Journal of the Atmospheric Sciences*, *78*(11), 3781–3797. https://doi.org/10.1175/jas-d-20-0337.1

Daleu, C. L., Plant, R., Woolnough, S., Stirling, A., & Harvey, N. (2020). Memory properties in cloud-resolving simulations of the diurnal cycle of deep convection. *Journal of Advances in Modeling Earth Systems*, *12*(8), e2019MS001897. https://doi.org/10.1029/2019ms001897

Dal Gesso, S., & Neggers, R. (2018). Can we use single-column models for understanding the boundary layer cloud-climate feedback? *Journal of Advances in Modeling Earth Systems*, *10*(2), 245–261. https://doi.org/10.1002/2017ms001113

Davies, L. (2008). Self-organisation of convection as a mechanism for memory (Unpublished doctoral dissertation). The University of Reading.

Davies, L., Plant, R., & Derbyshire, S. (2013). Departures from convective equilibrium with a rapidly varying surface forcing. *Quarterly Journal of the Royal Meteorological Society*, *139*(676), 1731–1746. https://doi.org/10.1002/qj.2065

Davies, L., Plant, R. S., & Derbyshire, S. H. (2009). A simple model of convection with memory. *Journal of Geophysical Research*, *114*, D17202. https://doi.org/10.1029/2008jd011653

Del Genio, A. D., Wu, J., Wolf, A. B., Chen, Y., Yao, M.-S., & Kim, D. (2015). Constraints on cumulus parameterization from simulations of observed MJO events. *Journal of Climate*, *28*(16), 6419–6442. https://doi.org/10.1175/jcli-d-14-00832.1

de Roode, S. R., Duynkerke, P. G., & Siebesma, A. P. (2000). Analogies between mass-flux and Reynolds-averaged equations. *Journal of the Atmospheric Sciences*, *57*(10), 1585–1598. https://doi.org/10.1175/1520-0469(2000)057<1585:abmfar>2.0.co;2

Emanuel, K. A. (1991). A scheme for representing cumulus convection in large-scale models. *Journal of the Atmospheric Sciences*, *48*(21), 2313–2329. https://doi.org/10.1175/1520-0469(1991)048<2313:asfrcc>2.0.co;2

Emanuel, K. A., & Živković-Rothman, M. (1999). Development and evaluation of a convection scheme for use in climate models. *Journal of the Atmospheric Sciences*, *56*(11), 1766–1782. https://doi.org/10.1175/1520-0469(1999)056<1766:daeoac>2.0.co;2

Gerard, L., Piriou, J.-M., Brožková, R., Geleyn, J.-F., & Banciu, D. (2009). Cloud and precipitation parameterization in a meso-gamma-scale operational weather prediction model. *Monthly Weather Review*, *137*(11), 3960–3977. https://doi.org/10.1175/2009mwr2750.1

Gettelman, A., Truesdale, J., Bacmeister, J., Caldwell, P., Neale, R., Bogenschutz, P., & Simpson, I. (2019). The single column atmosphere model version 6 (SCAM6): Not a scam but a tool for model evaluation and development. *Journal of Advances in Modeling Earth Systems*, *11*(5), 1381–1401. https://doi.org/10.1029/2018ms001578

Grandpeix, J.-Y., & Lafore, J.-P. (2010). A density current parameterization coupled with Emanuel's convection scheme. Part I: The models. *Journal of the Atmospheric Sciences*, *67*(4), 881–897. https://doi.org/10.1175/2009jas3044.1

Grandpeix, J.-Y., Lafore, J.-P., & Cheruy, F. (2010). A density current parameterization coupled with Emanuel's convection scheme. Part II: 1D simulations. *Journal of the Atmospheric Sciences*, *67*(4), 898–922. https://doi.org/10.1175/2009JAS3045.1

Guérémy, J. (2011). A continuous buoyancy based convection scheme: One-and three-dimensional validation. *Tellus A: Dynamic Meteorology and Oceanography*, *63*(4), 687–706. https://doi.org/10.1111/j.1600-0870.2011.00521.x

Haerter, J. O., Böing, S. J., Henneberg, O., & Nissen, S. B. (2019). Circling in on convective organization. *Geophysical Research Letters*, *46*(12), 7024–7034. https://doi.org/10.1029/2019gl082092

Hagos, S., Feng, Z., Plant, R. S., Houze, R. A., Jr., & Xiao, H. (2018). A stochastic framework for modeling the population dynamics of convective clouds. *Journal of Advances in Modeling Earth Systems*, *10*(2), 448–465. https://doi.org/10.1002/2017ms001214

Han, J., & Pan, H.-L. (2011). Revision of convection and vertical diffusion schemes in the NCEP global forecast system. *Weather and Forecasting*, *26*(4), 520–533. https://doi.org/10.1175/waf-d-10-05038.1

Han, Y., Zhang, G. J., Huang, X., & Wang, Y. (2020). A moist physics parameterization based on deep learning. *Journal of Advances in Modeling Earth Systems*, *12*(9), e2020MS002076. https://doi.org/10.1029/2020ms002076

Harvey, N. J., Daleu, C. L., Stratton, R. A., Plant, R. S., Woolnough, S. J., & Stirling, A. J. (2022). The impact of surface heterogeneity on the diurnal cycle of deep convection. *Quarterly Journal of the Royal Meteorological Society*, *148*(749), 3509–3527. https://doi.org/10.1002/qj.4371

Holloway, C. E. (2017). Convective aggregation in realistic convective-scale simulations. *Journal of Advances in Modeling Earth Systems*, *9*(2), 1450–1472. https://doi.org/10.1002/2017ms000980

Holloway, C. E., & Neelin, J. D. (2009). Moisture vertical structure, column water vapor, and tropical deep convection. *Journal of the Atmospheric Sciences*, *66*(6), 1665–1683. https://doi.org/10.1175/2008jas2806.1

Holloway, C. E., & Woolnough, S. J. (2016). The sensitivity of convective aggregation to diabatic processes in idealized radiative-convective equilibrium simulations. *Journal of Advances in Modeling Earth Systems*, *8*(1), 166–195. https://doi.org/10.1002/2015ms000511

Hong, S.-Y., & Lim, J.-O. J. (2006). The WRF single-moment 6-class microphysics scheme (WSM6). *Asia-Pacific Journal of Atmospheric Sciences*, *42*(2), 129–151.

Hong, S.-Y., Noh, Y., & Dudhia, J. (2006). A new vertical diffusion package with an explicit treatment of entrainment processes. *Monthly Weather Review*, *134*(9), 2318–2341. https://doi.org/10.1175/mwr3199.1

Hourdin, F., Grandpeix, J.-Y., Rio, C., Bony, S., Jam, A., Cheruy, F., et al. (2013). LMDZ5B: The atmospheric component of the IPSL climate model with revisited parameterizations for clouds and convection. *Climate Dynamics*, *40*(9), 2193–2222. https://doi.org/10.1007/s00382-012-1343-y

Hourdin, F., Rio, C., Grandpeix, J.-Y., Madeleine, J.-B., Cheruy, F., Rochetin, N., et al. (2020). LMDZ6A: The atmospheric component of the IPSL climate model with improved and better tuned physics. *Journal of Advances in Modeling Earth Systems*, *12*(7), e2019MS001892. https://doi.org/10.1029/2019MS001892

Hwong, Y.-L., Colin, M., Aglas-Leitner, P., Muller, C., & Sherwood, S. (2023). Data - Assessing memory in convection schemes using idealized tests (version 4) [Dataset]. Zenodo. https://doi.org/10.5281/zenodo.8073523

Hwong, Y.-L., Sherwood, S., & Fuchs, D. (2022). Can we use 1D models to predict 3D model response to forcing in an idealized framework? *Journal of Advances in Modeling Earth Systems*, *14*(4), e2021MS002785. https://doi.org/10.1029/2021ms002785

Hwong, Y.-L., Song, S., Sherwood, S., Stirling, A., Rio, C., Roehrig, R., et al. (2021). Characterizing convection schemes using their responses to imposed tendency perturbations. *Journal of Advances in Modeling Earth Systems*, *13*(5), e2021MS002461. https://doi.org/10.1029/2021ms002461

Iacono, M. J., Delamere, J. S., Mlawer, E. J., Shephard, M. W., Clough, S. A., & Collins, W. D. (2008). Radiative forcing by long-lived greenhouse gases: Calculations with the AER radiative transfer models. *Journal of Geophysical Research*, *113*, D13103. https://doi.org/10.1029/2008jd009944

Janjić, Z. I. (1994). The step-mountain eta coordinate model: Further developments of the convection, viscous sublayer, and turbulence closure schemes. *Monthly Weather Review*, *122*(5), 927–945. https://doi.org/10.1175/1520-0493(1994)122<0927:tsmecm>2.0.co;2

Jeevanjee, N., Hassanzadeh, P., Hill, S., & Sheshadri, A. (2017). A perspective on climate model hierarchies. *Journal of Advances in Modeling Earth Systems*, *9*(4), 1760–1771. https://doi.org/10.1002/2017ms001038

Jeevanjee, N., & Romps, D. M. (2013). Convective self-aggregation, cold pools, and domain size. *Geophysical Research Letters*, *40*(5), 994–998. https://doi.org/10.1002/grl.50204

Jiménez, P. A., Dudhia, J., González-Rouco, J. F., Navarro, J., Montávez, J. P., & García-Bustamante, E. (2012). A revised scheme for the WRF surface layer formulation. *Monthly Weather Review*, *140*(3), 898–918. https://doi.org/10.1175/mwr-d-11-00056.1

Kain, J. S. (2004). The Kain–Fritsch convective parameterization: An update. *Journal of Applied Meteorology*, *43*(1), 170–181. https://doi.org/10.1175/1520-0450(2004)043<0170:tkcpau>2.0.co;2

Khairoutdinov, M., Randall, D., & DeMott, C. (2005). Simulations of the atmospheric general circulation using a cloud-resolving model as a superparameterization of physical processes. *Journal of the Atmospheric Sciences*, *62*(7), 2136–2154. https://doi.org/10.1175/jas3453.1

Khairoutdinov, M., & Randall, D. A. (2001). A cloud resolving model as a cloud parameterization in the NCAR Community Climate System Model: Preliminary results. *Geophysical Research Letters*, *28*(18), 3617–3620. https://doi.org/10.1029/2001gl013552

Khouider, B., Biello, J., & Majda, A. J. (2010). A stochastic multicloud model for tropical convection. *Communications in Mathematical Sciences*, *8*(1), 187–216. https://doi.org/10.4310/cms.2010.v8.n1.a10

Kirsch, B., Ament, F., & Hohenegger, C. (2021). Convective cold pools in long-term boundary layer mast observations. *Monthly Weather Review*, *149*(3), 811–820. https://doi.org/10.1175/mwr-d-20-0197.1

Kruse, I. L., Haerter, J. O., & Meyer, B. (2022). Cold pools over The Netherlands: A statistical study from tower and radar observations. *Quarterly Journal of the Royal Meteorological Society*, *148*(743), 711–726. https://doi.org/10.1002/qj.4223

Mapes, B. (1997). Equilibrium vs. activation control of large-scale variations of tropical deep convection. In R. K. Smith (Ed.), *The physics and parameterization of moist atmospheric convection* (pp. 321–358). Kluwer Academic Publishers.

Mapes, B., & Neale, R. (2011). Parameterizing convective organization to escape the entrainment dilemma. *Journal of Advances in Modeling Earth Systems*, *3*(2), M06004. https://doi.org/10.1029/2011ms000042

Morcrette, J.-J. (1991). Radiation and cloud radiative properties in the European Centre for Medium Range Weather Forecasts forecasting system. *Journal of Geophysical Research*, *96*(D5), 9121–9132. https://doi.org/10.1029/89JD01597

Moseley, C., Hohenegger, C., Berg, P., & Haerter, J. O. (2016). Intensification of convective extremes driven by cloud–cloud interaction. *Nature Geoscience*, *9*(10), 748–752. https://doi.org/10.1038/ngeo2789

Muller, C., & Bony, S. (2015). What favors convective aggregation and why? *Geophysical Research Letters*, *42*(13), 5626–5634. https://doi.org/10.1002/2015gl064260

Muller, C., & Held, I. M. (2012). Detailed investigation of the self-aggregation of convection in cloud-resolving simulations. *Journal of the Atmospheric Sciences*, *69*(8), 2551–2565. https://doi.org/10.1175/jas-d-11-0257.1

Neggers, R., & Griewank, P. J. (2021). A binomial stochastic framework for efficiently modeling discrete statistics of convective populations. *Journal of Advances in Modeling Earth Systems*, *13*(3), e2020MS002229. https://doi.org/10.1029/2020ms002229

Neggers, R., & Griewank, P. J. (2022). A decentralized approach for modeling organized convection based on thermal populations on microgrids. *Journal of Advances in Modeling Earth Systems*, *14*(10), e2022MS003042. https://doi.org/10.1029/2022ms003042

Pan, D.-M., & Randall, D. D. (1998). A cumulus parameterization with a prognostic closure. *Quarterly Journal of the Royal Meteorological Society*, *124*(547), 949–981. https://doi.org/10.1002/qj.49712454714

Park, S. (2014a). A unified convection scheme (UNICON). Part I: Formulation. *Journal of the Atmospheric Sciences*, *71*(11), 3902–3930. https://doi.org/10.1175/jas-d-13-0233.1

Park, S. (2014b). A unified convection scheme (UNICON). Part II: Simulation. *Journal of the Atmospheric Sciences*, *71*(11), 3931–3973. https://doi.org/10.1175/jas-d-13-0234.1

Park, S., & Bretherton, C. S. (2009). The university of Washington shallow convection and moist turbulence schemes and their impact on climate simulations with the community atmosphere model. *Journal of Climate*, *22*(12), 3449–3469. https://doi.org/10.1175/2008jcli2557.1

Peters, K., Jakob, C., Davies, L., Khouider, B., & Majda, A. J. (2013). Stochastic behavior of tropical convection in observations and a multicloud model. *Journal of the Atmospheric Sciences*, *70*(11), 3556–3575. https://doi.org/10.1175/jas-d-13-031.1

Piriou, J.-M., Redelsperger, J.-L., Geleyn, J.-F., Lafore, J.-P., & Guichard, F. (2007). An approach for convective parameterization with memory: Separating microphysics and transport in grid-scale equations. *Journal of the Atmospheric Sciences*, *64*(11), 4127–4139. https://doi.org/10.1175/2007jas2144.1

Pritchard, M. S., Moncrieff, M. W., & Somerville, R. C. (2011). Orogenic propagating precipitation systems over the United States in a global climate model with embedded explicit convection. *Journal of the Atmospheric Sciences*, *68*(8), 1821–1840. https://doi.org/10.1175/2011jas3699.1

Qian, L., Young, G. S., & Frank, W. M. (1998). A convective wake parameterization scheme for use in general circulation models. *Monthly Weather Review*, *126*(2), 456–469. https://doi.org/10.1175/1520-0493(1998)126<0456:acwpsf>2.0.co;2

Randall, D. A., & Pan, D.-M. (1993). Implementation of the Arakawa-Schubert cumulus parameterization with a prognostic closure. In *The representation of cumulus convection in numerical models* (pp. 137–144). Springer.

Rio, C., Del Genio, A. D., & Hourdin, F. (2019). Ongoing breakthroughs in convective parameterization. *Current Climate Change Reports*, *5*(2), 95–111. https://doi.org/10.1007/s40641-019-00127-w

Rio, C., Grandpeix, J.-Y., Hourdin, F., Guichard, F., Couvreux, F., Lafore, J.-P., et al. (2013). Control of deep convection by sub-cloud lifting processes: The ALP closure in the LMDZ5B general circulation model. *Climate Dynamics*, *40*(9), 2271–2292. https://doi.org/10.1007/s00382-012-1506-x

Rio, C., & Hourdin, F. (2008). A thermal plume model for the convective boundary layer: Representation of cumulus clouds. *Journal of the Atmospheric Sciences*, *65*(2), 407–425. https://doi.org/10.1175/2007JAS2256.1

Rio, C., Hourdin, F., Couvreux, F., & Jam, A. (2010). Resolved versus parametrized boundary-layer plumes. Part II: Continuous formulations of mixing rates for mass-flux schemes. *Boundary-Layer Meteorology*, *135*(3), 469–483. https://doi.org/10.1007/s10546-010-9478-z

Rochetin, N., Couvreux, F., Grandpeix, J.-Y., & Rio, C. (2014). Deep convection triggering by boundary layer thermals. Part I: LES analysis and stochastic triggering formulation. *Journal of the Atmospheric Sciences*, *71*(2), 496–514. https://doi.org/10.1175/JAS-D-12-0336.1

Rochetin, N., Grandpeix, J.-Y., Rio, C., & Couvreux, F. (2014). Deep convection triggering by boundary layer thermals. Part II: Stochastic triggering parameterization for the LMDZ GCM. *Journal of the Atmospheric Sciences*, *71*(2), 515–538. https://doi.org/10.1175/JAS-D-12-0337.1

Rooney, G. G., Stirling, A. J., Stratton, R. A., & Whitall, M. (2022). C-pool: A scheme for modelling convective cold pools in the met office unified model. *Quarterly Journal of the Royal Meteorological Society*, *148*(743), 962–980. https://doi.org/10.1002/qj.4241

Sakradzija, M., Seifert, A., & Dipankar, A. (2016). A stochastic scale-aware parameterization of shallow cumulus convection across the convective gray zone. *Journal of Advances in Modeling Earth Systems*, *8*(2), 786–812. https://doi.org/10.1002/2016ms000634

Sakradzija, M., Seifert, A., & Heus, T. (2015). Fluctuations in a quasi-stationary shallow cumulus cloud ensemble. *Nonlinear Processes in Geophysics*, *22*(1), 65–85. https://doi.org/10.5194/npg-22-65-2015

Schlemmer, L., & Hohenegger, C. (2016). Modifications of the atmospheric moisture field as a result of cold-pool dynamics. *Quarterly Journal of the Royal Meteorological Society*, *142*(694), 30–42. https://doi.org/10.1002/qj.2625

Shamekh, S., Lamb, K. D., Huang, Y., & Gentine, P. (2023). Implicit learning of convective organization explains precipitation stochasticity. *Proceedings of the National Academy of Sciences*, *120*(20), e2216158120. https://doi.org/10.1073/pnas.2216158120

Siebesma, A. P., Soares, P. M., & Teixeira, J. (2007). A combined eddy-diffusivity mass-flux approach for the convective boundary layer. *Journal of the Atmospheric Sciences*, *64*(4), 1230–1248. https://doi.org/10.1175/jas3888.1

Skamarock, W. C., Klemp, J. B., Dudhia, J., Gill, D. O., Barker, D. M., Duda, M. G., et al. (2008). *A description of the advanced research WRF*. Version, 3. National Center for Atmospheric Research.

Skamarock, W. C., Klemp, J. B., Dudhia, J., Gill, D. O., Liu, Z., Berner, J., et al. (2019). *A description of the advanced research WRF model version 4* (Vol. 145, p. 145). National Center for Atmospheric Research.

Stephens, G. L., L'Ecuyer, T., Forbes, R., Gettelmen, A., Golaz, J.-C., Bodas-Salcedo, A., et al. (2010). Dreary state of precipitation in global models. *Journal of Geophysical Research*, *115*, D24211. https://doi.org/10.1029/2010jd014532

Stevens, B., & Bony, S. (2013). What are climate models missing? *Science*, *340*(6136), 1053–1054. https://doi.org/10.1126/science.1237554

Tan, Z., Kaul, C. M., Pressel, K. G., Cohen, Y., Schneider, T., & Teixeira, J. (2018). An extended eddy-diffusivity mass-flux scheme for unified representation of subgrid-scale turbulence and convection. *Journal of Advances in Modeling Earth Systems*, *10*(3), 770–800. https://doi.org/10.1002/2017ms001162

Tobin, I., Bony, S., Holloway, C. E., Grandpeix, J.-Y., Seze, G., Coppin, D., et al. (2013). Does convective aggregation need to be represented in cumulus parameterizations? *Journal of Advances in Modeling Earth Systems*, *5*(4), 692–703. https://doi.org/10.1002/jame.20047

Tompkins, A. M. (2001). Organization of tropical convection in low vertical wind shears: The role of cold pools. *Journal of the Atmospheric Sciences*, *58*(13), 1650–1672. https://doi.org/10.1175/1520-0469(2001)058<1650:ootcil>2.0.co;2

Tompkins, A. M., & Semie, A. G. (2017). Organization of tropical convection in low vertical wind shears: Role of updraft entrainment. *Journal of Advances in Modeling Earth Systems*, *9*(2), 1046–1068. https://doi.org/10.1002/2016ms000802

Torri, G., & Kuang, Z. (2016). Rain evaporation and moist patches in tropical boundary layers. *Geophysical Research Letters*, *43*(18), 9895–9902. https://doi.org/10.1002/2016gl070893

Torri, G., Kuang, Z., & Tian, Y. (2015). Mechanisms for convection triggering by cold pools. *Geophysical Research Letters*, *42*(6), 1943–1950. https://doi.org/10.1002/2015gl063227

Villalba-Pradas, A., & Tapiador, F. J. (2022). Empirical values and assumptions in the convection schemes of numerical models. *Geoscientific Model Development*, *15*(9), 3447–3518. https://doi.org/10.5194/gmd-15-3447-2022

Wing, A. A., & Emanuel, K. A. (2014). Physical mechanisms controlling self-aggregation of convection in idealized numerical modeling simulations. *Journal of Advances in Modeling Earth Systems*, *6*(1), 59–74. https://doi.org/10.1002/2013ms000269

Wing, A. A., Stauffer, C. L., Becker, T., Reed, K. A., Ahn, M.-S., Arnold, N. P., et al. (2020). Clouds and convective self-aggregation in a multi-model ensemble of radiative-convective equilibrium simulations. *Journal of Advances in Modeling Earth Systems*, *12*(9), e2020MS002138. https://doi.org/10.1029/2020ms002138

Xu, K.-M., & Randall, D. A. (1998). Influence of large-scale advective cooling and moistening effects on the quasi-equilibrium behavior of explicitly simulated cumulus ensembles. *Journal of the Atmospheric Sciences*, *55*(5), 896–909. https://doi.org/10.1175/1520-0469(1998)055<0896:iolsac>2.0.co;2

Yamada, T. (1983). Simulations of nocturnal drainage flows by a q2l turbulence closure model. *Journal of the Atmospheric Sciences*, *40*(1), 91–106. https://doi.org/10.1175/1520-0469(1983)040(0091:SONDFB)2.0.CO;2

Yanai, M., Esbensen, S., & Chu, J.-H. (1973). Determination of bulk properties of tropical cloud clusters from large-scale heat and moisture budgets. *Journal of the Atmospheric Sciences*, *30*(4), 611–627. https://doi.org/10.1175/1520-0469(1973)030<0611:dobpot>2.0.co;2

Yanase, T., Nishizawa, S., Miura, H., Takemi, T., & Tomita, H. (2020). New critical length for the onset of self-aggregation of moist convection. *Geophysical Research Letters*, *47*(16), e2020GL088763. https://doi.org/10.1029/2020gl088763

Yano, J.-I., & Plant, R. (2012). Convective quasi-equilibrium. *Reviews of Geophysics*, *50*, RG4004. https://doi.org/10.1029/2011rg000378

Zhang, C., & Wang, Y. (2017). Projected future changes of tropical cyclone activity over the western north and south pacific in a 20-km-mesh regional climate model. *Journal of Climate*, *30*(15), 5923–5941. https://doi.org/10.1175/jcli-d-16-0597.1

Zhang, G., & McFarlane, N. (1995). Sensitivity of climate simulations to the parameterization of cumulus convection in the Canadian Climate Centre general circulation model. *Atmosphere-Ocean*, *33*(3), 407–446. https://doi.org/10.1080/07055900.1995.9649539

Zuidema, P., Torri, G., Muller, C., & Chandra, A. (2017). A survey of precipitation-induced atmospheric cold pools over oceans and their interactions with the larger-scale environment. *Surveys in Geophysics*, *38*(6), 1283–1305. https://doi.org/10.1007/s10712-017-9447-x